# MAGNETIC RARE EARTH COMPOUNDS



Howlett-Packard Company
Palo Alto, California 94304

## SEMIANNUAL TECHNICAL REPORT

December 1970

Contract No. DAAH01-70-C-1106
Program Code No. 0D10



ARP Division
Research and Engineering Directorate
U.S. Army Missile Command
Redstone Arsenal, Alabama

A Research Project Sponsored by the Advanced Research Project Agency, Department of Defense, Washington, D.C., ARPA Order 1627

NOTICE

"This research was sponsored by the Advanced Research Projects Agency of the Department of the Defense under ARPA Order 1627 and was monitored by the US Army Missile Command under Contract Number DAAH01-70-C-1106. Views and conclusions expressed herein are the primary responsibility of the author or the contractor and should not be interpreted as representing the official opinion or policy of USAMICOM, ARPA, DOD or any other agency of the Government."

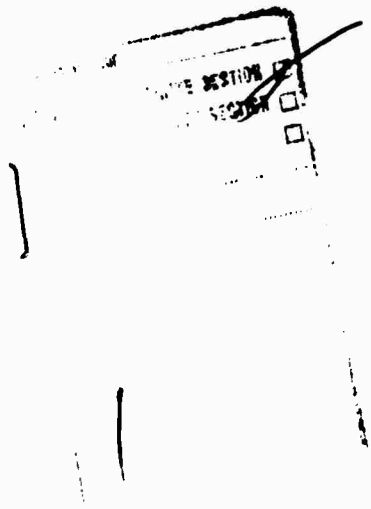

TECHNICAL REQUIREMENT NO. 1335
ARPA Order 1627

# MAGNETIC RARE EARTH COMPOUNDS

SEMIANNUAL TECHNICAL REPORT

December 1970

HEWLETT-PACKARD
COMPANY
Palo Alto, California
94304

Contract No. DAAH01-70-C-1106
Program Code No. OD10

ARP Division
Research and Engineering Directorate
U. S. Army Missile Command
Redstone Arsenal, Alabama

A Research Project Sponsored by the Advanced Research Project Agency, Department of Defense, Washington, D.C., ARPA Order 1627

TABLE OF CONTENTS

TABLE OF CONTENTS

## LIST OF FIGURES

## LIST OF FIGURES

## LIST OF TABLES

# FOREWORD

This interim report describes the work performed under contract DAAH01-70-C-1106 for the ARP Division, Research and Engineering Directorate, U.S. Army Missile Command, Redstone Arsenal, Alabama, during the period 1 June 1970 through 30 November 1970. The monitor for this project was G. W. Hagood. The work was performed in the Solid State Laboratory of Hewlett-Packard Laboratories, and this report was written by R.A. Burmeister, T.L. Felmlee and R. Hiskes.

## SUMMARY

A steady-state crystal growth system suitable for the growth of magnetic rare earth compounds has been designed, constructed, and successfully operated. The system has a number of important features: a) it provides a thermally stable crystal growth environment, b) it provides a means for readily moving the seed crystal (or a substrate in the case of epitaxial growth) in and out of the solution, which prevents freezing the crystal in the solution upon cooling, c) it provides a large solution surface (2½" diameter) so that growth can be performed on large substrates in the case of epitaxial growth, and d) it incorporates a stirring mechanism which can ensure a homogeneous solution and enhance transport of crystal constituents to the growing crystal.

A very stable solvent, consisting of $BaO\text{-}B_2O_3\text{-}BaF_2$, has been developed. This solvent is nonvolatile and nonreactive, and is well suited to the solution growth of magnetic materials. Its unique qualities make it particularly advantageous for controlled epitaxial growth of mixed orthoferrites or garnets. Characterization of this solvent has been initiated, and the experimental solubility curve for $YFeO_3$ indicates that 30 molar percent will dissolve at a typical crystal growth temperature of 1300°C.

Extensive characterization studies of the $YFeO_3$ crystals grown in the steady-state unit are in progress. Equipment built for these studies includes apparatus for observing straight domain walls and the interaction of defects with these domain walls, as well as apparatus for generating and moving bubble domains. Arrays of bubbles have been generated in $YFeO_3$ grown in the $BaO-B_2O_3-BaF_2$ solvent, and the coercivity and mobility of crystals grown from this solvent have been measured and found comparable to the best values for crystals grown in the PbO-based solvents.

Emission spectrographic analysis indicates that $YFeO_3$ crystals grown in the BaO-based solvent contain only trace amounts of boron and $\sim$0.08 wt.% barium, which is lower than the value of 0.29wt.% Pb reported for $YFeO_3$ in the PbO based solvent. [40]

Lang topographic studies have revealed defects in $YFeO_3$ which cannot be seen optically, and this technique is proving to be a very useful characterization tool.

## 1.0. INTRODUCTION

Since magnetic bubble domains have become potential candidates for efficient information storage as described by Bobeck[1] in 1967, they have generated a great deal of technological interest, primarily because of the capability they offer for high storage density (up to $10^9$ bits per cubic inch of memory). Additional features of this technology include the ability to perform logic and memory in the same material, low power requirements and nonvolatility. The bright promise of the bubble domain, however, is tempered by the very demanding materials requirements for practical devices. Some of the stringent requirements for usable material include:

1. thin single crystal platelets with the easy axis of magnetization perpendicular to the surface of the platelet;
2. very low defect density over large areas of the platelet, since nearly all the common defects of crystals severely restrict domain wall motion;
3. domains generated in such materials must be small enough to allow high storage densities, yet large enough to be detectable ($1\mu <$ diameter $< 75\mu$ ), they must be mobile, and the magnetic properties of the material must be temperature insensitive to operating temperature;

At present there are three classes of magnetic materials in which cylindrical magnetic domains have been observed:

1. hexagonal ferrites,
2. rare earth orthoferrites,
3. mixed rare earth garnets.

The hexagonal ferrites, such as $PbFe_{12}O_{19}$ have disappointingly low intrinsic bubble mobilities[2] and are not of practical interest at present. The orthoferrites, in general, have bubble diameters that are somewhat large ($\sim$ 25-75$\mu$) for efficient device use, but have the highest mobilities. The recently reported uniaxial garnets[3] have bubble diameters and mobilities in the right range, but the origin of their uniaxiality is not yet known, and is probably not an intrinsic property of the crystal.

In the past, a great deal of research in the area of the growth and characterization of magnetic rare earth compounds has been built upon an art-based technology. For example, most crystal growth processes used for these materials are based on a molten salt slow-cooling solution growth technique using a PbO-based solvent developed nearly two decades ago by Remeika.[4] In spite of numerous disadvantages

of the PbO-based solvent and the slow cooling technique itself, many investigators continue to utilize this combination for the growth of rare earth compounds, and although minor refinements have been added, there have been very few innovations in materials preparation (with a few notable exceptions).[5-13]

As materials requirements become more stringent, the conventional growth techniques become inadequate, since they are essentially uncontrolled and generally produce polycrystalline growth with poor crystalline quality. Frequently only very small portions of crystals are suitable for device studies. Also, some of the mixed garnets being considered for bubble devices contain up to six different metallic cations, which somehow must be distributed uniformly over large regions of the crystal. The amount of incorporation of each cation depends upon the ratio of its concentration in a saturated liquid in thermodynamic equilibrium with the solid garnet. The ratio of the concentration in the liquid to that in the solid is termed its distribution coefficient ($K_o = X_s / X_\ell$), which quite often is a complicated function of temperature. Since a homogeneous crystal requires the distribution coefficients of each of the constituent cations to remain constant with time, it is obvious that a slow cooling procedure must inevitably produce inhomogeneties, which indeed have been detected by many investigators.[14,15]

It is clear from the discusion above that materials problems are the major limitation to the practical utilization of bubble devices. In view of the technological importance of these devices and the key role of magnetic rare earth compounds, this program was undertaken in an effort to advance the state of the art in the science and technology of these materials. The specific objectives of this program include the following:

1. Development of practical techniques for the growth of single crystals of rare earth compounds having properties suitable for studies and utilization of magnetic domain wall phenomena ("bubble" motion).

2. Acquisition of the necessary data to better characterize and quantitatively describe both the crystal growth process and the salient physical and chemical properties of the crystals produced.

3. Determination of the relationships between methods and parameters of the crystal growth process and the relevant physical properties of the crystals thus grown.

To date, efforts have centered on the first two objectives. Techniques have been developed for the growth of high quality $YFeO_3$ crystals which are generally applicable to any class of "bubble" materials. These crystals are being characterized in an effort to understand interrelationships between their magnetic and other physical properties. The groundwork has thus been laid for correlation between growth parameters and the relevant physical properties of the crystals, which will allow optimization of preparative techniques for these crystals.

The choice of material for the development and characterization of the growth process was somewhat arbitrary since the solution growth of both orthoferrites and garnets is similar, and it is not yet clear which particular material is best suited for ultimate device application. $YFeO_3$ was chosen as the initial material to be studied in this program, since it is similar in many respects to the balance of the rare earth orthoferrites and thus can be considered typical. Furthermore, it is probably the best characterized "bubble" material currently available. For example, it has been shown that $YFeO_3$ exhibits an exceptionally high domain wall mobility (intrinsic mobility rather than the defect limited mobility generally observed

in all other orthoferrites). Also, the $Y^{3+}$ ion has no magnetic moment, and hence, the problem of separating the effects of impurity substitutions or other point imperfections on the $Fe^{3+}$ sublattice are simplified. The only significant disadvantage of $YFeO_3$ is the relatively large bubble diameter ($\sim 100\mu m$).

In this program we have investigated the use of steady-state solution growth techniques, in which the crystal grows, usually on a seed, at a constant (time invariant) temperature, nourished by a source of material in a different (hotter) region of the melt. Material is thus continually transported down the temperature gradient to the growing interface. This technique obviates the homogeneity problems found in the transient (slow-cool) techniques, and provides the best means for reliable control of the parameters which enhance crystal quality and morphology. Liquid epitaxial growth may be regarded as a sub-class of seeded solution growth, but has not generally been applied to this class of materials for several reasons, most notably the lack of a suitable substrate and the unavailability of a stable, nonvolatile, nonreactive solvent. Recently, a few suitable substrates have been found, such as $Gd_3Ga_5O_{12}$ for the growth of $Y_3Fe_5O_{12}$, and $YAlO_3$ for the growth

of $YFeO_3$, and successful liquid epitaxial growth has been reported by several investigators.[5, 6] However, none of these studies used steady-state techniques.

The generality and applicability of results obtained in this program to other bubble material will become apparent in the following sections.

## 2.0. CRYSTAL GROWTH

### 2.1. General Considerations

There are several general requirements which must be fulfilled in crystal growth of magnetic rare earth compounds to be able to use them effectively in "bubble" devices. The first of these is the exceptionally high degree of crystalline perfection which must be obtained. The need for this is illustrated by the coercive force associated with various common crystal defects listed in Table I.[16] A second stringent requirement is that relatively large areas (1 cm x 1 cm or larger) of highly perfect material are required to store a useful amount of data. A third requirement is that the crystals must be relatively thin (5 - 100 $\mu$m) to maintain stable cylindrical domains.[1] Another requirement is that the material must be oriented with the easy axis of magnetization perpendicular to the plane of the crystal platelet. A fifth requirement is homogeneity of composition and magnetic properties of the crystal, the latter being strongly dependent on the first. An additional requirement is that the crystals produced should contain a minimum of strain and/or foreign impurities. Strain in these crystals leads to high coercivities, and foreign impurities to variations in the magnetic properties. Finally, the process used to grow magnetic rare earth materials should be easily controllable and reproducible. This requirement is of utmost importance with regard to the development of routine production capability.

TABLE I

Coercive Forces Associated with Common Crystal Defects.

| DEFECTS | COERCIVE FORCE |
|---|---|
| 110 Twin Planes | 1000 Oe |
| Grain Boundaries($\theta \geq 0.1°$) | 100 $\theta^2$ Oe |
| Scratches and Etch Pits | 1 - 10 Oe |
| Inclusions and Voids | 1 - 50 Oe |
| Growth Plane Intersection | 1 - 50 Oe |
| Dislocations | $\sim$ 1 Oe |
| Growth Striations | 0 - 50 Oe |

(from Reference 16)

2.1.1. Discussion of Available Techniques

Methods used to grow magnetic rare earth crystals in the past have included conventional flux growth techniques, hydrothermal solution growth,[8] Bridgman growth,[13] the floating zone technique,[12] a modified Czochralski technique using a solution rather than the congruent melt,[7] and chemical vapor phase deposition.[10] However, there are limitations associated with each of these methods.

The operating temperature of the chemical vapor deposition process is rigidly dictated by the thermodynamics of the chemical reactions involved, which generally occur over a very limited range of temperatures. This very narrow temperature regime makes it difficult to control the composition of mixed rare earth orthoferrites and garnets, and it is fortuitous if the operating temperature coincides with the optimum growth temperature.

The principal difficulties associated with the growth of magnetic rare earth materials by the hydrothermal method are (a) the low growth rate[8] which makes it too slow for the practical growth of bulk crystals, (b) the requirement for elaborate equipment, and (c) incorporation of hydroxyl ions by the crystal.

Neither the Bridgman nor the floating zone techniques can be used to grow iron garnet crystals because they are incongruently melting.[17,18] The orthoferrites are congruently melting, but the melting points are very high (~ 1670°C for $YFeO_3$), creating apparatus requirements that are difficult

to reliably maintain for any appreciable length of time, and in addition, a high oxygen pressure (> 1 atm) is required. Another limitation for the Bridgman technique is that for each crystal growth run, the platinum crucible used to contain the growth melt must be sacrificed.

The bulk of the magnetic rare earth crystals grown to date have been grown by a random-nucleation, slow-cooled (transient), PbO-based solution technique.[3, 15] There are several problems associated with this method which relate to the nature of the solvent, the lack of control of nucleation, and the fact that the crystal growth occurs over a wide range of temperatures (usually > 200°C) during the cooling. These disadvantages will be discussed further in Section 2.1.4.

Techniques have been developed for the solution growth of rare earth garnets which solve problems inherent in the randomly nucleated growth process. For example, Bennett[9] and Tolksdorf[19] describe the crystal growth of YIG on a seed attached to a platinum crucible which is capable of being rotated to remove the seed from the melt. This crystal growth technique is efficient because it avoids the many small crystals grown by the random nucleation technique, and permits the use of one melt for many crystal growth runs. The seeded steady-state technique has many superior features which will be discussed in greater detail in the following section.

### 2.1.2. Crystal Growth by the Seeded Steady-State Solution Technique

To circumvent the problems inherent in methods generally used previously in crystal growth of rare earth orthoferrites and garnets, we have

utilized the seeded steady-state solution technique in this program. This technique has not been investigated in detail by others, except as noted above. The steady-state solution technique is, in essence, growth in a thermal gradient. The growth occurs at constant temperature on a seed crystal held in a cool portion of a solution which is saturated by a source of crystal constituents in a hot zone of the same solution.

Probably the most important advantage of solution growth is that it allows one to select the temperature best suited to the phase equilibria of any particular type of material, thus avoiding problems of the type encountered in the Bridgman and floating zone technique described in Section 2.1.1. Magnetic rare earth materials can be grown by the steady-state solution technique at temperatures of 850-1300°C with conditions at the higher end of the range being the better suited for crystal growth, for serveral reasons. The viscosity of the solvent is much lower, thus promoting transport of material to the crystal; the kinetics of crystal growth are much faster than at lower temperatures, increasing the growth rate, and due to the slope of the liquidus, the solution is more enriched in crystal constituents at the higher temperature than at the lower temperatures, thus requiring less transport of material (less solute material has to be rejected) through the crystal-liquid interfacial region during growth.

A second distinct advantage of seeded steady-state solution growth is that it provides an effective way to homogeneously mix cations in the crystal lattice, which is essential for growing high quality solid solutions.

A third important advantage of seeded steady-state growth is that it can readily be used to grow magnetic materials epitaxially on a nonmagnetic substrate material. This eliminates many problems associated with the bulk growth of crystals as discussed in Section 2.1.1., including a number of lengthy processing steps, and would provide a means of handling and supporting these materials as very thin layers, which is the form in which they will be used in device application.

In addition to these advantages, the use of a seed or substrate in combination with steady-state growth permits the control of nucleation in the solvent, thus reducing any tendency to dendritic growth. This is a serious problem in transient growth, and leads to crystals containing a large number of solvent inclusions. Seeded growth also provides for control of orientation, making it possible to reproducibly grow crystals with the easy axis of magnetization parallel to the direction of crystal growth, thus eliminating the growth of material which cannot be used. The use of a seed also provides a means of growing large crystals in relatively small systems compared to some used in the transient or slow-cooling technique.[11]

Steady-state solution growth is a relatively simple technique, and therefore, is easily and reliably controlled. A number of reports of garnet and other iron containing crystals grown by this method attest to this.[9,21-27]

### 2.1.3. Seed or Substrate Selection

There are several considerations in selecting seed or substrate materials to be used in the steady-state growth of this class of materials. To permit epitaxial growth of the magnetic material on the substrate, the lattice

parameters of the two materials must be nearly the same, and to prevent the separation of the new growth from the seed on cooling, the coefficients of thermal expansion must be similar. In addition, lattice parameters and coefficients of thermal expansion of the substrate must be matched to those of the magnetic material to prevent the creation of lattice strain which would produce a high coercivity in the material. For application considerations, the seed should have a large cross-sectional area since this is a limiting factor in the amount of information that can be stored. The seed should also be nonmagnetic to allow free bubble movement and it is desirable (but not necessary) that it be transparent so that the Faraday technique can be used to detect the location of bubbles in the material. $YAlO_3$ is a possible substrate for $YFeO_3$, since it meets some of the above requirements and is available in large area single crystal form.

### 2.1.4. Solvent Considerations

A review of a number of reports [15, 28-30] of growth of magnatic rare earth materials by transient PbO-based solvent techniques as well as prior experimental work of our own, indicates that this solvent has a number of inherent disadvantages. They are:

a. the solvent is very corrosive toward the crucible material (platinum) at growth temperatures;

b. the solution is fairly volatile, and thus the composition and the surface level of the liquid change throughout the crystal growth unless a sealed system is employed. Also, in epitaxial growth processes, the substrate may be damaged before the epitaxial growth begins, as a result of the vapor transport of PbO to the substrate surface;

c. in addition to the orthoferrites or garnets, large quantities of other phases crystallize out, thus consuming source material for the magnetic materials; and

d. the solvent is more dense than the magnetic material, making seeded steady-state growth difficult.

The problems associated with the PbO-based solvent may be largely circumvented by use of the $BaO-B_2O_3$ solvent system.[5] The advantages of this system are numerous. First, there is no corrosive attack on the crucible material (platinum) by the solvent, which permits (a) very long growth runs to be carried out, (b) several runs to be carried out using the same solution, and (c) minimization of the amount of platinum in solution which might be incorporated by the crystal. A second advantage of the BaO-based solvent is that loss by vaporization is negligible. This is important for epitaxial growth, since it allows growth without a change in the liquid level. The third advantage is its high solubility for $YFeO_3$, which means that during crystal growth the ratio

of the concentration of the crystal constituent in the liquid to that in the solid is high and, therefore, growth conditions are highly favorable. Another advantage of the BaO-based flux is its low viscosity [31] which allows easier transport of crystal constituents from source to crystal. An additional advantage is that the solution is less dense than the crystal, and thus the source material rests on the bottom of the crucible where it cannot interfere with the growth of the crystal. This is an important asset for epitaxial growth.

An analysis of the lead-based solvents is given in the Appendix, but here we direct our attention to the more interesting BaO-based solvents. The solvent power in this system arises from the combination of an ionic liquid, such as BaO, with a network liquid like $B_2O_3$. Linares[5] found that upon slow cooling solutions of YIG-BaO-$B_2O_3$, the iron content of the stable precipitating phase increased as the ratio $B_2O_3$/BaO increased; and that as the amount of $B_2O_3$ increased from 25 - 50 mole %, the stable phase varied from $YFeO_3 \rightarrow Y_3Fe_5O_{12} \rightarrow BaO \cdot 6Fe_2O_3 \rightarrow Fe_2O_3$ (see Figure 1). Apparently, the $Y^{3+}$ enters the network structure of the borate more readily than the $Fe^{3+}$, which, because it is excluded, is more readily available to the growing crystal. [32] As the liquid, then, becomes less ionic, its dissolving power for $Fe^{3+}$ becomes weaker, hence the amount of $Fe^{3+}$ in the growing phase is greater. Because of this tendency of the solvent to preferentially dissolve one crystal constituent over another (in

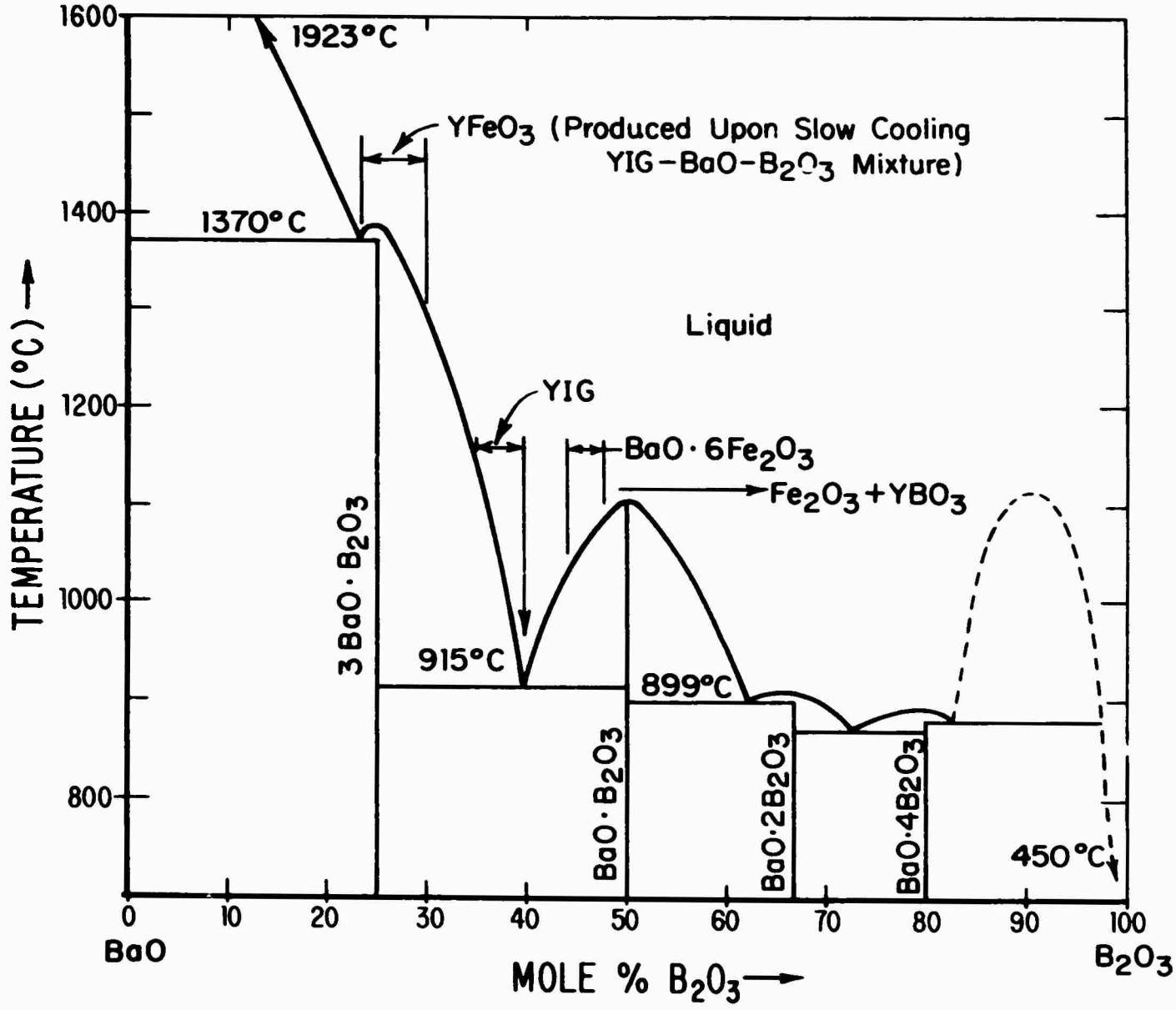


Figure 1. $BaO-B_2O_3$ Phase Diagram Depicting Stability Regions for Various Magnetic Materials.[5]

this case the addition of $Ba^{2+}$ causes $Fe^{3+}$ to be dissolved preferentially to $Y^{3+}$), it is desirable to be able to tailor the properties of the solvent to fit the crystal to be grown in it. This binary solvent was ideal for the growth of YIG, since it is most stable at the low melting eutectic at 39.5% $B_2O_3$. Several investigators have used the solvent since it was first discovered,[22, 31] but there have been no recent reports of its use.

Although $YFeO_3$ could be grown from the eutectic $BaO-B_2O_3$ mixture by adding enough $Y_2O_3$ and $Fe_2O_3$ to make an equimolar mixture, the solution would then be (during growth) saturated in $Y_2O_3$ but unsaturated in $Fe_2O_3$, which would make the theoretical yield as well as the velocity of growth less than optimum, and would be deleterious to mass transport in the solution.

In light of these considerations, it was decided to examine possible additions to the $BaO-B_2O_3$ solvent which would make it more amenable to the crystal growth of $YFeO_3$. One such addition is $BaF_2$, which allows the ionic character and melting range of the solvent to be shifted to more desirable values, and also appears to decrease the viscosity of the solvent. It is particularly advantageous to provide $F^-$ in the melt because it has been noted[33] that $PbF_2$ added to the PbO-based melts enhances the growth of large single crystals, possibly by suppressing the formation of $Fe^{4+}$ in the crystal. $Fe^{4+}$ is formed when $Pb^{2+}$ replaces $Y^{3+}$ accompanied by a change in valence of $Fe^{3+}$ to $Fe^{4+}$. $F^-$ provides the necessary charge

compensation by replacing $O^{2-}$. $BaF_2$ has a very low vapor pressure at crystal growth temperatures,[34] and therefore, the stability of the solvent is unimpaired. An experimental program has been initiated to characterize the $BaO-B_2O_3-BaF_2$ ternary system in order to determine the optimum regions for crystal growth.

$BaO-B_2O_3-BaF_2$ is not the only stable solvent system that can be used. Linares[5] pointed out a number of possible substitutions for BaO and $B_2O_3$; and alternatives to $BaF_2$ which are presently being examined are the other barium halides, such as $BaCl_2$, $BaBr_2$ or $BaI_2$. $Cl^-$, $Br^-$, and $I^-$ are all much larger than $F^-$ and should not be as likely to substitute for $O^{2-}$ in the $YFeO_3$ lattice. Thermodynamic data for these compounds suggest that they should all be stable at crystal growth temperatures.

2.1.4.1. Interface Stability Analysis

It is appropriate at this point to consider the maximum rate of growth that one may expect in crystals grown from this solution while still maintaining the integrity and quality of the product. It is well established that the cores of solution-grown orthoferrites and garnets often contain inclusions and growth faults[14,15] which are indicative of dendritic growth caused by an excessive growth velocity. A high quality single crystal, free from inclusions and inhomogeneities, requires a stable planar interface during growth. An estimate of the maximum velocity beyond which a planar interface will break down into a cellular interface can be obtained by a

constitutional supercooling analysis. Tiller[35] has shown that the critical velocity for a multicomponent solution is given by

$$V_{max} = \frac{G_L}{\sum_i \left\{ \frac{\frac{\partial \bar{T}_L}{\partial X^i} (k_o^{\,i} - 1)\, X^i(0)}{D^i} \right\}} \qquad (1)$$

where $i$ = crystal components ($Y_2O_3$ and $Fe_2O_3$),

$\bar{T}_L$ = liquidus temperature

$G_L$ = temperature gradient in the liquid at the interface

$k_o^{\,i}$ = distribution coefficient for component i

$D^i$ = liquid diffusion coefficient for component i

$X^i(0)$ = interface concentration of component i.

The distribution coefficient is given by

$$k_o^{\,i} = \frac{\rho_{compd.}}{\rho_{liquid}} \frac{\sum_{j=1}^{n} X_j W_j}{\sum_{j=1}^{2} X_j W_j} \begin{matrix} \text{liquid} \\ \text{compd.} \end{matrix} \frac{X^i_{compd.}}{X^i_{liquid}} \qquad (2)$$

where $\rho$ = density

$X$ = mole fraction

$W$ = molecular weight.

In Equation 1 , it is assumed that

(1) there is no convection in the liquid so that all mass transport takes place by diffusion,

(2) interface attachment kinetics are infinite,

(3) interfacial energy is zero, and

(4) temperature gradient in the solid is equal to that in the liquid.

Both surface energy ($\gamma > 0$) and interface attachment ($\mu < \infty$) effects resist interface breakdown, so that the maximum allowable velocity is increased by amounts $\Delta V_\gamma$ and $\Delta V_\mu$. Convection reduces the critical velocity as does a reduced temperature gradient in the solid (one would expect $G_s \sim 0$ for an optically transparent material like $YFeO_3$). The critical velocity is given by

$$V_C < V_{max}^{c.s.c.} + \Delta V_T + \Delta V_C + \Delta V_\gamma + \Delta V_\mu \qquad (3)$$

where $V_{max}^{c.s.c.}$ is calculated from Equation 1,

$\Delta V_T < 0$ results from thermal effects,

$\Delta V_C < 0$ results from convection in the liquid,

$\Delta V_\gamma > 0$ is a surface energy effect, and

$\Delta V_\mu > 0$ is an interface kinetic effect.

Each of these effects may be large, but they tend to cancel each other, and there is no data available to evaluate them. Only an estimate, then, of the allowable interface velocity is obtainable from Equation 1.

In order to calculate $V_{max}$, the system parameters must be calculated or estimated. $G_L$, the temperature gradient in the liquid, is chosen to be 1.8°C/cm in the steady-state growth situation (a typical experimental value). The magnitude of the diffusion coefficients of components in the solution can be estimated from viscosity data with the aid of the Stokes-Einstein Relation†

$$D = KT/6\pi\eta r, \tag{4}$$

where K = Boltzmann's constant

T = temperature (°K)

$\eta$ = viscosity

r = ionic radius.

Oliver[36] has measured viscosities in PbO-based solvents and has fit the data to an equation of the form

$$\eta = Ae^{E/RT}, \tag{5}$$

where, for a PbO-48 mole % $PbF_2$ solution

†This relation is strictly valid only when ions of the diffusing species are much larger than those of the solvent, but it will provide a useful estimation here.

$$A = 0.0026 \pm 0.00005,$$

$$B = 5.4 \pm 1.1 \quad .$$

This leads to $D \sim 10^{-5}$ cm$^2$/sec at 1300°C, a value similar to most metal systems. Since the viscosity of the BaO-based solvents is less than that of the PbO-based solvent used in the calculations,[31] this value of D represents a lower limit for the diffusion coefficients of crystal components in this solvent. The slope of the liquidus surface is at a minimum along the $YFeO_3$-solvent join if this is a quasi-binary system, the maximum component of the slope being along this join (the slope is zero perpendicular to this join). Since velocity is maximized by minimizing the liquidus slope, it is advantageous to grow crystals along the join. The slope of this line for the solvent composition used in the steady-state growth experiment has been obtained experimentally and found to be $m_L = 816$°C/mole fraction at 1300°C. The components of the liquidus slopes in the direction of the crystal components will therefore be in the range $0 < \left|\partial \bar{T}_L / \partial X^1\right| < 816$°C/mole fraction, and for convenience we choose $\left|\partial \bar{T}_L / \partial X^1\right| = 400$°C/mole fraction (only the order of magnitude is important for this calculation). The density of the compound is 5.67 gm/cc, and the density of the liquid has been found to be 4.75 gm/cc. At 1300°C (the interface temperature), the interface concentration is given by the equilibrium concentration of saturated liquid ($X_{YFeO_3} = 0.3$ mole fraction) divided by the distribution coefficient in Equation 2.

For growth of $YFeO_3$ from a typical BaO-based solvent containing equi-molar amounts of $Fe_2O_3$ and $Y_2O_3$, the distribution coefficients become (from Equation 2)

$$k_o^{\,i} = 3.98 \qquad i = Y_2O_3,\ Fe_2O_3\ ,$$

and the maximum velocity calculated from Equation 1 is $V_{max} = 3.28 \times 10^{-7}$ cm/sec. To avoid constitutional supercooling leading to interface breakdown and a dendritic mode of growth, the steady-state growth experiment should therefore be designed for a growth velocity of $\sim 10^{-7}$ cm/sec.

This velocity is several orders of magnitude lower than the maximum allowable velocity in growth from a pure melt, but is comparable to values computed by Tiller for solution growth of several classes of semiconductors from a binary solution (which range from $10^{-6}$ to $10^{-10}$ cm/sec). It should be noted that $V_{max}$ increases strongly as the growth temperature increases; and hence it is advantageous from this point of view to have the interface temperature as high as possible, commensurate with apparatus capabilities and other requirements.

## 2.2. Experimental

### 2.2.1. Growth of Seed Crystals

#### 2.2.1.1. Procedure

The method of growth of seed crystals required for the steady-state solution growth was similar to that outlined by Wanklyn.[28] This method was chosen because it was easy to implement, it gave reproducible results, and the crystals were adequate in size for use as seeds. The materials used were from various suppliers and have the following purity levels: $Y_2O_3$ - 99.9999%; $B_2O_3$ and $Fe_2O_3$ - 99.999%; PbO and $PbF_2$ - 99.99%. The starting materials were weighed to give mixtures with the composition shown in Table II and were thoroughly mixed. The mixtures were loaded into platinum crucibles which were loosely covered and set into a muffle furnace.

The source materials, $Fe_2O_3$ and $Y_2O_3$, were dissolved at the soak temperature and the temperature was lowered at a constant, slow rate to the final temperature indicated in Table II. A slow stream of air was continuously pumped into the muffle to maintain an appreciable oxygen pressure and to remove PbO and $PbF_2$ vapors from the interior of the furnace since they attack the alumina lining. At the final temperature, the crucibles were quickly removed from the furnace, tipped to pour the solvent out and replaced in the furnace. The temperature of the furnace was then

## TABLE II

**Growth Parameters and Results for Transient Growth Runs used to Produce Seed Crystals.**

| Run No. | Initial Compositions Mole % | | | | | Soak Time Hr. | Soak Temp. °C | Cooling Rate °C/hr | Final Temp. °C | Initial Charge wt/gm | Wt. Loss in run gm | Phases Present | $YFeO_3$ % Yield |
|---|---|---|---|---|---|---|---|---|---|---|---|---|---|
| | PbO | $PbF_2$ | $B_2O_3$ | $Fe_2O_3$ | $Y_2O_3$ | | | | | | | | |
| 7 | 43.5 | 25.7 | 5.8 | 11.3 | 13.7 | 18.5 | 1278 | 2.0 | 800 | 88.7 | 17.4 | YOF, $YFeO_3$ | 67.1 |
| 8 | " | " | " | " | " | 15.6 | 1280 | 2.0 | 920 | 175.6 | 20.8 | YOF, $YFeO_3$ | 50.3 |
| 9 | " | " | " | " | " | 12.8 | 1285 | 2.0 | 805 | 399.2 | 32.5 | YOF, YIG $YFeO_3$ | -- |
| 10 | " | " | " | " | " | 14.8 | 1286 | 2.3 | 788 | 351.1 | 42.9 | YOF, YIG | -- |
| 11 | " | " | " | " | " | " | " | " | " | 175.6 | 31.0 | YOF, $YFeO_3$ | 66.1 |

lowered (much faster than during crystal growth) to approximately 400°C where the crystals could be removed without cracking from thermal shock. The solvent still adhering to the crystals was removed by dissolving it in 20% $HNO_3$. In each run a considerable amount of YOF was formed.

2.2.1.2. Seed Crystal Growth Results

Typical crystals grown by this technique are shown in Figure 2. The conditions and results are summarized in Table II.

The low yield of $YFeO_3$ in No. 8, compared to Nos. 7 and 11, arises from the fact that this run was terminated at a much higher temperature than the others.

The formation of YOF in runs similar to these has been experienced by others.[28,37] The YOF is the first phase to crystallize from the solution as is indicated by the fact that it forms a crust at the surface of the solution and the magnetic crystals are found adhering to this crust. This formation is both an advantage and a disadvantage in the growth of $YFeO_3$. It helps in that it provides a nucleation site for the $YFeO_3$. Thus the amount of supersaturation is low when the $YFeO_3$ starts to grow and the tendency to dendritic growth is less; but on the other hand, a number of these sites are created leading to a large number of rather small crystals.

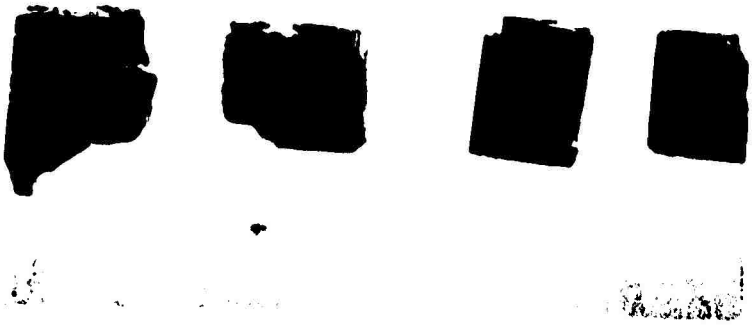

1 small div. = 1 mm

Figure 2. $YFeO_3$ Seed Crystals Grown from PbO-Based Solvent.

Another disadvantage in the formation of YOF is that it leads, indirectly, to the formation of YIG ($Y_3Fe_5O_{12}$) rather than $YFeO_3$. This can be explained by means of a set of competing chemical reactions.*

1. $Y_2O_3 + PbF_2 \rightleftarrows 2\ YOF + PbO$,
2. $3\ Y_2O_3 + 5\ Fe_2O_3 \rightleftarrows 2Y_3Fe_5O_{12}$, and
3. $Y_2O_3 + Fe_2O_3 \rightleftarrows 2YFeO_3$.

The formation of YOF in reaction 1 depletes the yttrium content in the solution. In the instance where this lowers the ratio Y/Fe (which was initially 1.21) to a sufficiently low value, reaction 2 becomes favored over reaction 3 and YIG is formed rather than $YFeO_3$. Another factor which contributes at least partially to this indirect formation of YIG is the concentration of $PbF_2$ in reaction 1. In cases where the weight loss, which is primarily due to loss of $PbF_2$,[29] is proportionately small, a higher $PbF_2$ concentration results; and the tendency toward YIG formation appears to be higher.

As depicted in Figure 2, the typical $YFeO_3$ crystal grown by this method is nearly cubic, measuring 3 - 4 mm on a side and is quite suitable for use as a seed crystal. There are, however, a number of voids and inclusions in these crystals which limit the areas suitable for device applications to dimensions of approximately 3 mm × 3 mm. These crystal

*It could best be explained by using a quaternary phase diagram, but the data necessary to construct such a diagram has not been completely determined. The explanation given above is only a qualitative one since there are a number of factors involved in fixing the ratio Y/F which are difficult to describe and measure.

defects are the direct result of dendritic growth which is brought on by supercooling the solution.

### 2.2.2. Preparation of Source Material

The materials used for this were $Y_2O_3$ and $Fe_2O_3$ powders described in the previous section. The powders were weighed out to give an equimolar mixture of the compounds and thoroughly mixed by grinding them together in an agate mortar. The mixed powders were pressed into a pellet die 3/8" in diameter. The pressed pellets, contained by an alumina boat, were then sintered at 1225°C for 20 hours in air, reground, repelleted and fired again at 1300°C for 48 hours. X-ray powder diffraction analysis indicated that all but approximately 5% of the starting materials had reacted to form $YFeO_3$. An emission spectrographic analysis showed the pellets to contain less than 50 ppm impurities. The density was 53% of the theoretical density for $YFeO_3$.

### 2.2.3. Characterization of the $BaO-B_2O_3-BaF_2$ Solvent

#### 2.2.3.1. Liquidus Surface and Solubility of $YFeO_3$

As $BaF_2$ is added to the eutectic mixture of BaO-39 5 mole % $B_2O_3$, the liquidus point becomes a curve in the ternary diagram as shown in Figure 3 . The experimental points in this diagram were determined by continuously monitoring the temperature of a solvent melt of known composition, and noting the temperature at which the solvent became too viscous to pour. The experiments were conducted in a muffle furnace, and once a reasonably low melting composition was found (such as 41 mole % BaO, 41 mole % $B_2O_3$, 18 mole % $BaF_2$), solubility determinations of $YFeO_3$ were conducted in the same furnace. Here, small crystals of $YFeO_3$ were suspended by a platinum wire in the nearly saturated melt, held for several hours, removed and examined optically. Either

(1) the solution was unsaturated and the crystal melted or developed rounded corners, or

(2) the solution was supersaturated and the crystal grew, as did a myriad of smaller crystals which nucleated both on the seed and on the platinum wire.

The solubility curve obtained in this fashion is shown in Figure 4 . The data can be fit to an equation of the form

$$x = x_o e^{-\Delta H/RT} \qquad (6)$$

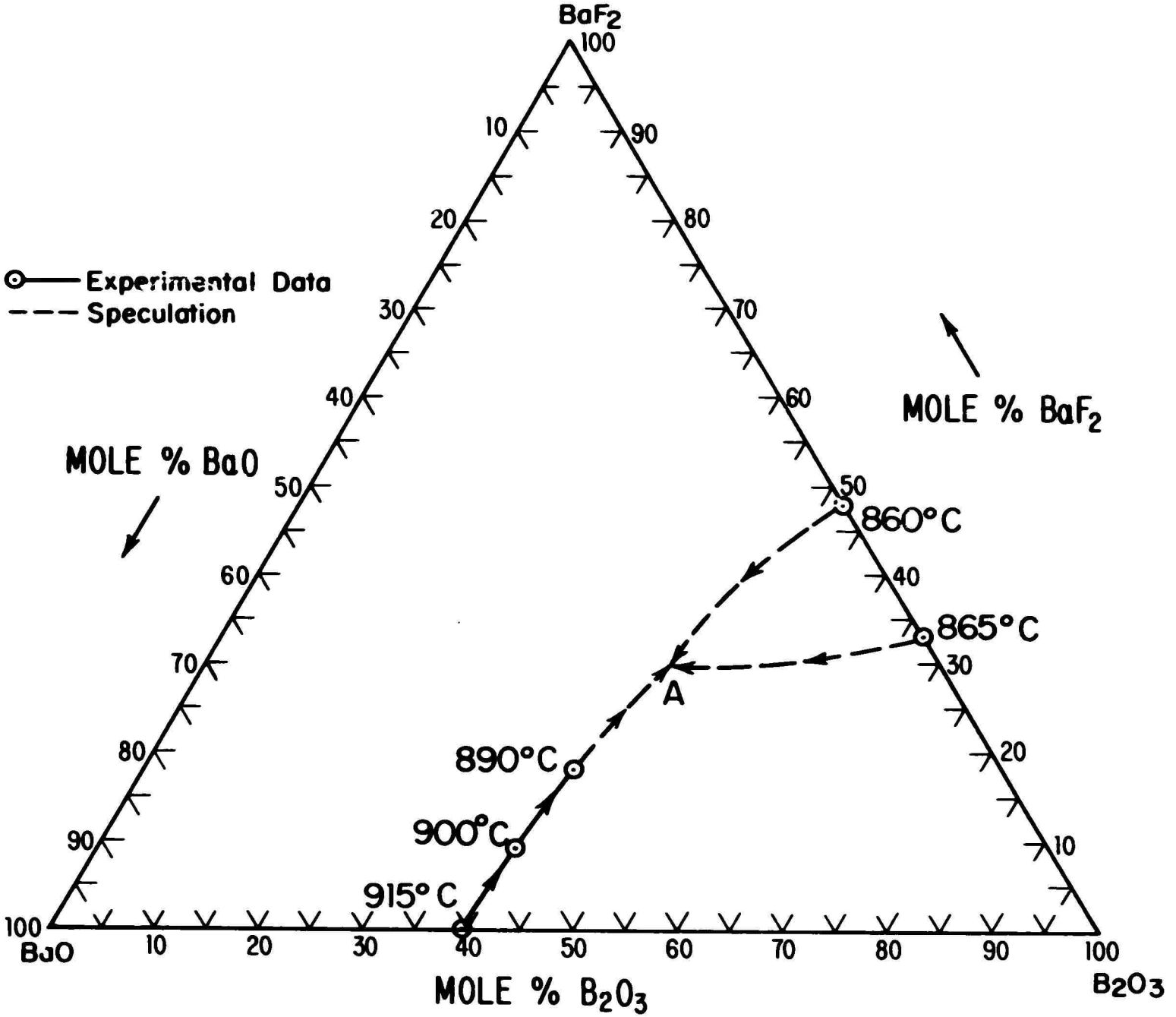


Figure 3. Possible Partial Liquidus Projection for $BaO \cdot B_2O_3 \cdot BaF_2$ System, with a Ternary Eutectic at A.

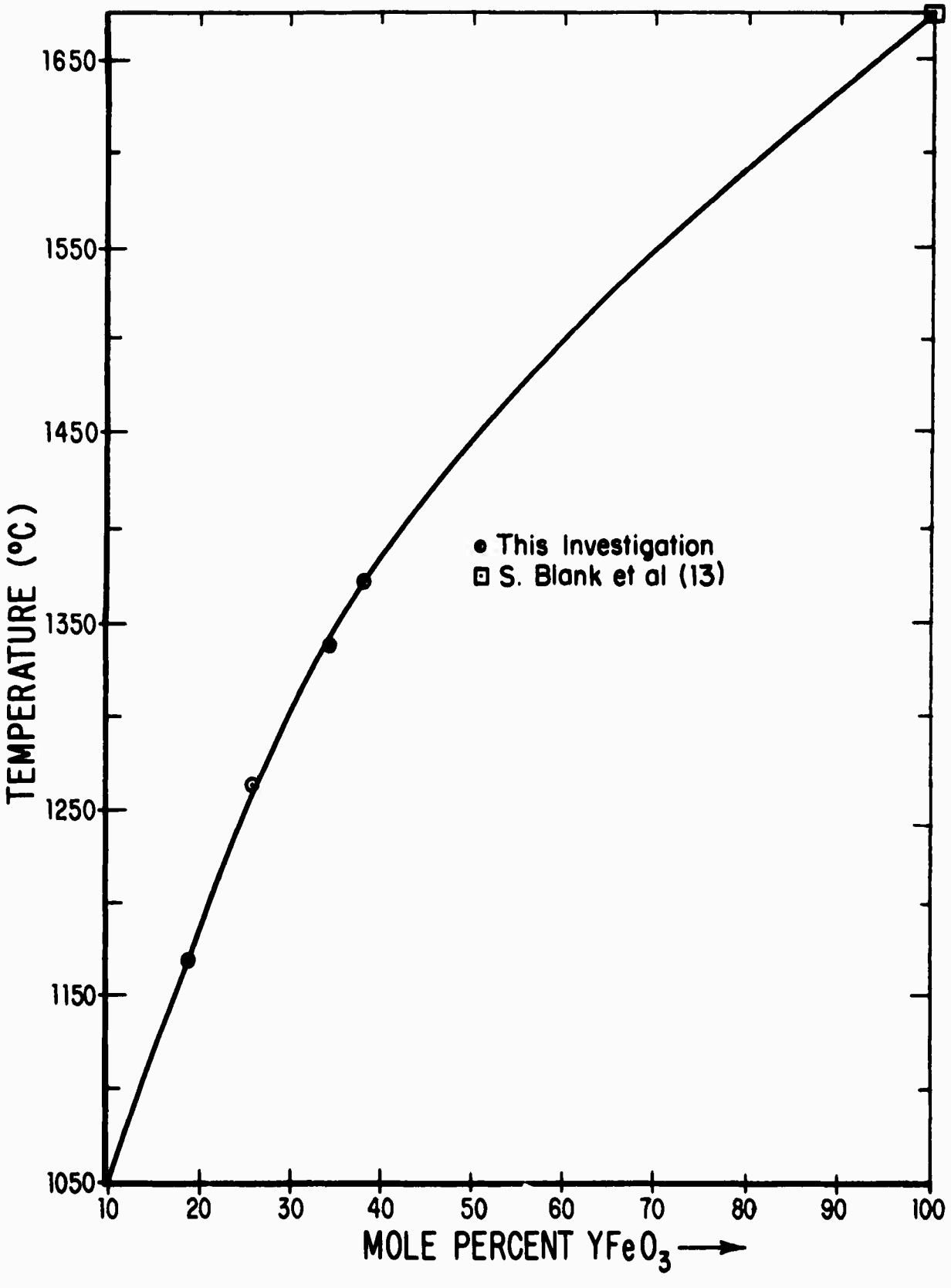


Figure 4. Solubility Curve for $YFeO_3$ in 41 (Mole) % BaO, 41% $B_2O_3$, 18 % $BaF_2$.

where $x_o = 5.03$ and $\Delta H = 19,408$ are assumed constant over a fairly wide range of temperature.

2.2.3.2. Density of the Solvent

The density of this solvent was determined with the aid of a recording electrobalance. A furnace placed vertically under the balance contains the saturated solvent, and a single crystal of $YFeO_3$ is suspended by a platinum wire from the balance. The weight of the crystal in air is recorded as it hangs just above the melt, and then the furnace is raised so that the crystal is completely immersed in the solvent. The buoyant force tends to reduce the apparent mass, but this is counteracted by a large downward force from surface tension effects on the Pt wire. If the melt is not saturated, the crystal will change in weight, and this weight change is related to the density by the equation

$$\Delta M_s = \Delta M_a \left[ 1 - \frac{\rho_s}{\rho_c} \right] \qquad (7)$$

where $\Delta M_s$ = change in apparent mass of the crystal in the solvent,

$\Delta M_a$ = change in mass of the crystal in air,

$\rho_s$ = density of solvent, and

$\rho_c$ = density of crystal.

This method for density determination is particularly advantageous because the effect of surface tension is eliminated when only changes in the apparent mass are considered. The density of the solvent calculated from the

weight change data is 4.75 ± 0.2 gm/cc, comparable to the calculated density (4.95 gm/cc) based on a weighted average of the densities of all the components.

2.2.4. Steady-state crystal growth

2.2.4.1. Apparatus

There were several important crystal growth requirements which necessitated special apparatus design considerations. It was necessary to be able to vary both the growth parameters and the operational procedures with a minimum of inconvenience.

Probably the most important of the growth parameters is the thermal environment of the growth system. The temperature must be constant with time, and its spatial distribution must be such that the seed crystal is the coolest part of the system so that growth will be on the seed rather than in any other part of the system.

Features of the system include a) a stirring mechanism which enhances growth by promoting transport of crystal constituents to the seed; b) a means of changing the level of the seed during growth so that it is easy to grow on the seed for a specified length of time and c) a large liquid surface exposure which provides the capability of growing on a large surface area seed. These last two features are especially advantageous for epitaxial growth on a substrate. Another feature of the apparatus is that crystals can be removed from the system at a rate slow enough to prevent cracking by thermal shock, which has been a serious problem in the growth of garnet crystals.[38] Finally, the design had to provide an apparatus that was reliable and gave reproducible results. A schematic view of the system is shown in Figure 5 . The furnace is a two-zone resistance

type with platinum - 40% rhodium windings and is capable of running continuously at 1540°C. The power supply for the furnace is controlled by a closed loop control system containing a current-adjusting type controller in conjunction with a silicon controlled rectifier unit.

Radiation shields and the solvent crucible are supported by alumina tubes which are terminated at the furnace ends by solid alumina plugs. A check of the temperature stability showed it to be adequate (±0.5°C at 1200°C) for crystal growth purposes.

2.2.4.2. Run Procecedure

The $Y_2O_3$, $Fe_2O_3$, and $B_2O_3$ were the same as that described earlier (see Section 2.2.1.1). The $BaF_2$ used was 99.9% pure with strontium being the only impurity present in any significant amount (200 ppm). The BaO was obtained by thermal decomposition of $BaCO_3$ which was 99.999% pure. The solvent materials were weighed out to give the composition indicated in Table III.

A solution saturated with $YFeO_3$ was mixed and loaded into a platinum crucible. $YFeO_3$ source material was dropped into the solution and a seed crystal was mounted on the end of a rod which could rotate the seed continuously in the solution. For all runs, the crystal was oriented so that the easy axis of magnetization was parallel to the axis of rotation.

The crystal growth parameters are indicated in Table III.

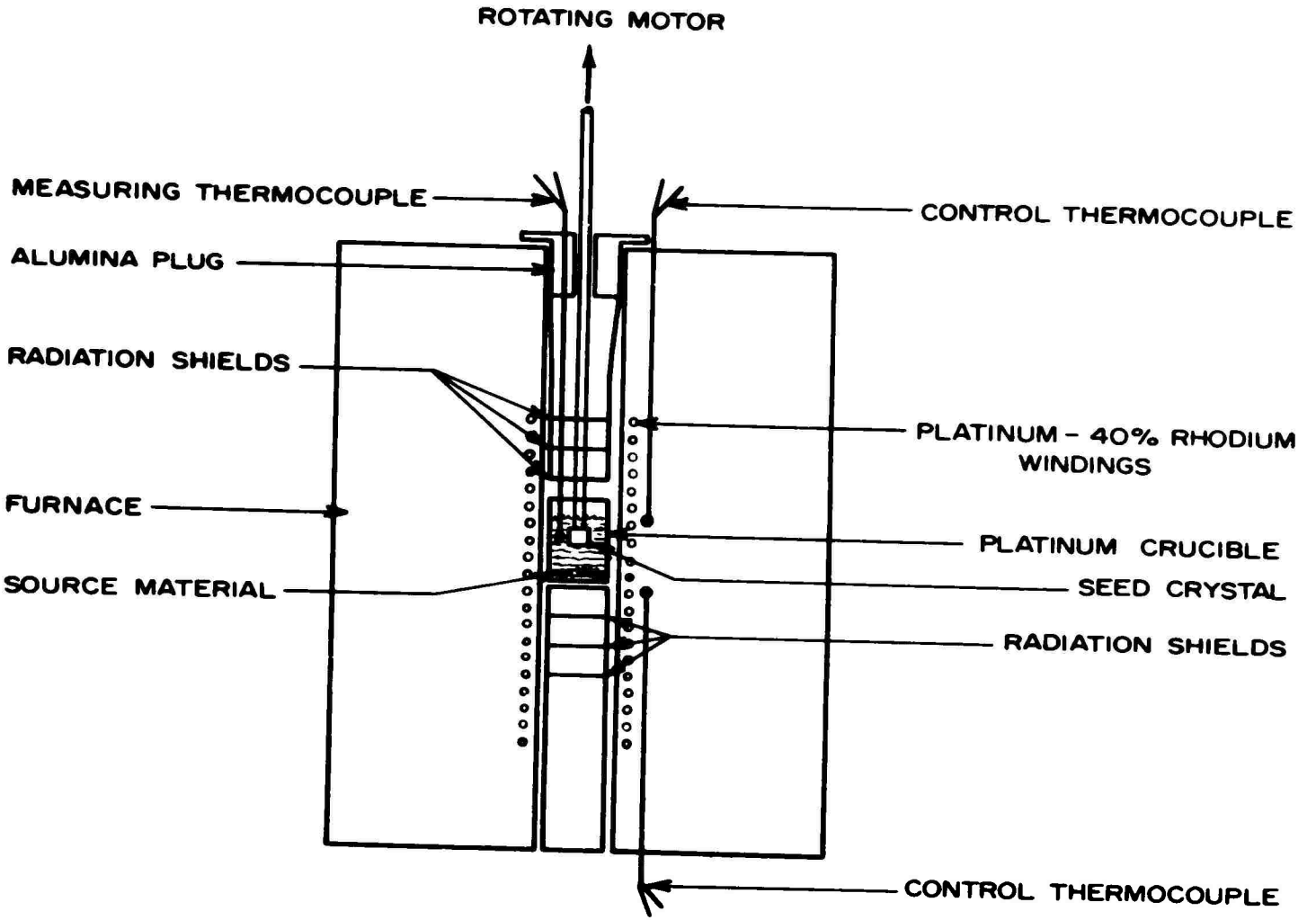


Figure 5. Schematic of Steady-State Crystal Growth System.

## TABLE III

Growth Parameters for Seeded, Steady-State Growth Runs of $YFeO_3$.

| Run No. | Composition of Solvent (mole percent) BaO | $B_2O_3$ | $BaF_2$ | Seed Temperature °C | Temperature Gradient from Source to Seed, °C/cm | Rotation Rate rpm | Run Time hrs. |
|---|---|---|---|---|---|---|---|
| SS1 | 53.4 | 35.6 | 11.1 | 1112 | 3.9 | 22 | 46 |
| SS2 | 53.4 | 35.6 | 11.1 | 1115 | 7.6 | 50 | 168 |
| SS3 | 53.4 | 35.6 | 11.1 | 1110 | 5.0 | 50 | 167 |
| SS4 | 53.4 | 35.6 | 11.1 | 1110 | 3.4 | 50 | 235 |
| SS5 | 42.6 | 41.0 | 16.4 | 1293 | 1.8 | 50 | 65 |
| SS6 | 42.6 | 41.0 | 16.4 | 1294 | 1.2 | 50 | 212 |

2.2.4.3. Results and discussion of steady-state solution growth

In each of the runs listed in TableIII, $YFeO_3$ was successfully grown onto the seed crystal with the exception of Run SS5, in which a crystal nucleated and grew on the platinum tube.

The first four runs can be discussed as a group. Emission spectrographic analysis of three separate samples indicates barium incorporation of approximately 0.08 wt. %. The new growth in Run SS4 has the same orientation (determined by the direction of easy magnetization) as the seed,indicating that the new growth was epitaxial to the seed crystal. The crystal growth,which measured 8 mm x 6 mm x 6 mm, was sliced with a 0.005" wire saw, mounted onto a polishing block, polished to a smooth finish and microscopically examined. The examination showed that the crystal growth contained a number of voids, grain boundaries and twin planes.

The crystal grown in Run SS5 measured 2 mm x 2.5 mm x 1 mm,and the easy axis of magnetization was normal to the flat side of the crystal. The morphology of the crystal grown under this set of conditions was very much better than for the first four runs. The approximate growth rate for SS5 was $1.1 \times 10^{-6}$ cm/sec as compared that of $4.7 \times 10^{-8}$ cm/sec for run SS4.

For run SS6, a stirring paddle was placed between the source and seed to assure homogeneity throughout the solution. A very large amount of material was transported to the seed proving that indeed this could be accomplished, but apparently the rate of transport exceeded that for stable growth,resulting in the growth being polycrystalline. The morphology of the small crystals was good (as in run SS5) indicating that with the proper crystal constituent transport conditions, good quality $YFeO_3$ crystals can be grown by this technique.

## 3.0. CHARACTERIZATION AND EVALUATION

### 3.1. Chemical Analyses

To determine the amount of impurities incorporated in the crystals grown in the BaO-based solvent as well as those from the PbO-based solvent, emission spectrographic analyses were performed on the crystals. Table IV shows typical impurity levels found in $YFeO_3$ samples grown from the PbO-based solvent and the BaO-Based solvent. To remove solvent inclusions, the samples were ground by mortar and pestle and soaked in a hot 20% $HNO_3$ solution for three hours. The Ba content appears to be lower for crystals grown in BaO-based solvents than the Pb content of those grown in PbO-based solvents, although further clarification is necessary.

TABLE IV

Typical Impurity Levels Found in $YFeO_3$ Samples Grown from PbO- and BaO-Based Solvents.

| Sample from PbO-based solvent | | Sample from BaO-based solvent | |
|---|---|---|---|
| Pb | 0.1-0.2 wt.%* | Ba | 0.08 wt. % |
| Al | < 2 ppm | Al | < 10 ppm |
| Ca | < 2 ppm | Ca | < 20 ppm |
| Si | 4-5 ppm | Si | ~ 200 ppm |
| Sr | < 10 ppm | Sr | < 400 ppm |

*Preliminary values prior to preparation of a suitable Pb standard for this analysis. Values as high as 0.29 wt.% have also been reported in the literature.[40]

3.2. Lattice Parameter Determinations

Geller[39] has indicated that there is a large (0.02 Å) variation in lattice parameters of the orthorhombic unit cell of $YFeO_3$ samples prepared under different conditions. To investigate the possibility that there may be a systematic variation in lattice parameter, an effort has been made to accurately determine values for samples prepared under different conditions. Lattice parameter considerations are also important in epitaxial growth experiments since lattice strain between old and new growth is related to the difference in lattice parameters. X-ray powder diffraction patterns were taken using a Debye-Scherrer camera, copper $K\alpha_1$ radiation, and a thin sheet (0.003") of aluminum foil to reduce fogging of the film by flourescent scattering. To avoid introducing absorption error into the determination, only the high angle lines were measured. A computer program by Evans et.al.,[41] was used to index the diffraction lines and compute least squares fitted lattice parameters. A few preliminary measurements confirm the discrepancies that Geller found. Samples of $YFeO_3$ prepared by sintering mixtures of $Y_2O_3$ and $Fe_2O_3$ powders (see Section 2.2.2.) differ in their lattice parameters (0.02-0.05 Å) from those prepared by the transient, PbO-based solution technique (see Section 2.2.1.2). There are at least two possible reasons for this sort of variation to exist. These are: a) the substitution of solvent ions for the ions in the compound, i.e., $F^-$ for $O^{2-}$ and, b) oxygen deficiencies combined with reduction of $Fe^{3+}$ to $Fe^{2+}$. The reasons for these discrepancies are not apparent. Since our preliminary measurements confirm Geller's original findings, this investigation will be extended.

## 3.3. Néel Temperature Determination

In the early stages of this investigation, a positive, non-destructive means of identifying whether the magnetic crystals obtained were $YFeO_3$ or some other compound, such as YIG or magnetoplumbite, was required. Accordingly, apparatus was set up to determine the Néel point of the crystals. The apparatus consists of a Cahn Type RH automatic recording electro-microbalance, a solenoid, a furnace, a measuring thermocouple and a regulated dc power supply. (See Figure 6 .) The microbalance is sensitive to a change in mass of one microgram and the solenoid produces a flux density of 12 gauss with a current of one ampere.

The sample is suspended from the balance approximately 5mm above the level of the upper turn of the coil with the measuring thermocouple placed 2mm below the sample pan. To carry out the determination, the temperature of the sample is raised at 3°C/min as the magnetic force on the sample is monitored by the balance. At the Néel point there is a sharp decrease in the force pulling the sample down. The Néel point of $YFeO_3$ determined by this technique was found to be 378°C, which can be compared to 372°C determined by Treves[42] from measurement of the magnetic moment. This is within experimental error since the Néel point is a gradual transition.

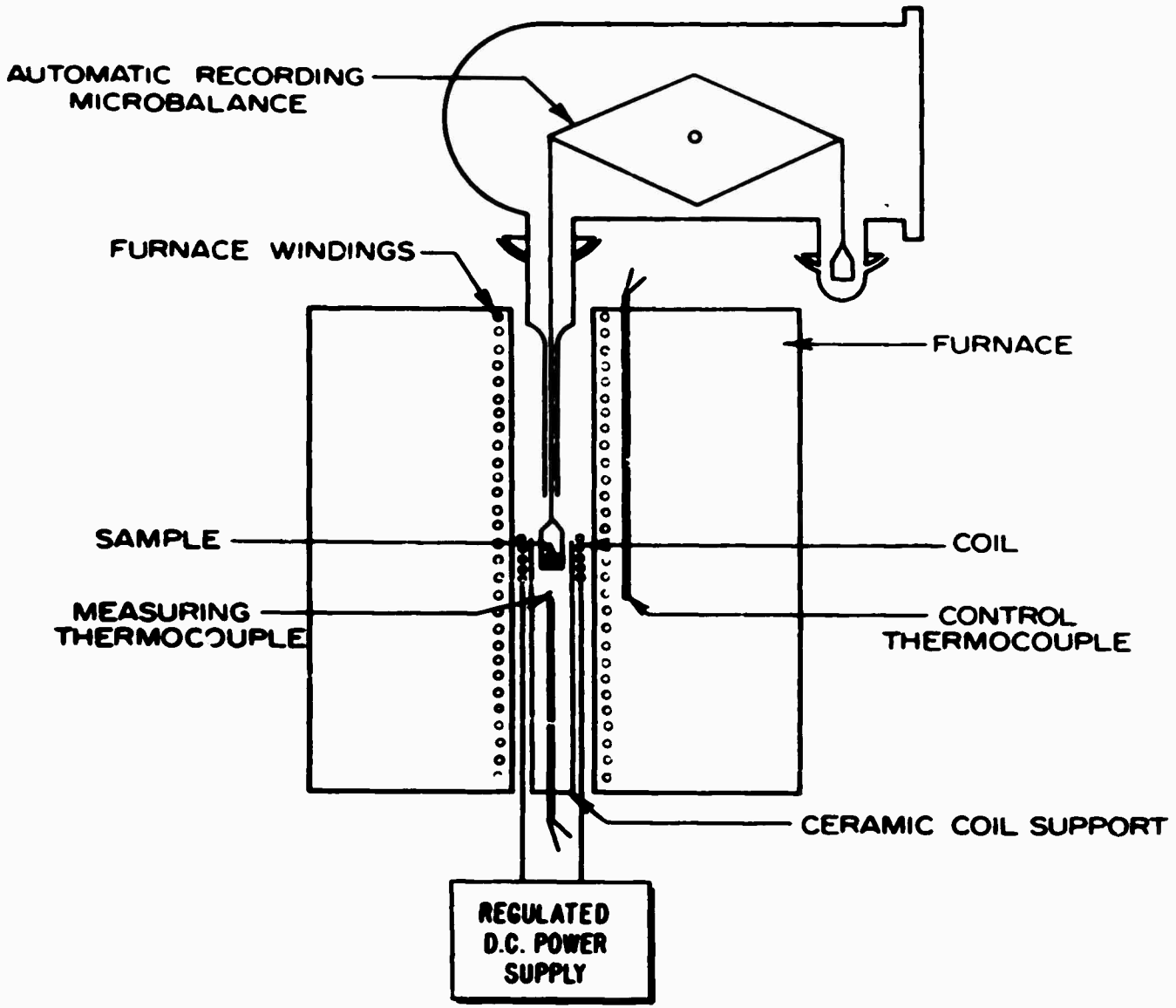


Figure 6. Apparatus for Néel Temperature Determination.

## 3.4. Straight Magnetic Domain Wall Apparatus

To evaluate platelets of $YFeO_3$ with respect to their defect concentration, apparatus was constructed which could readily reveal gross defects such as voids, inclusions, and grain boundaries, and could provide a means of observing the movement of a straight magnetic domain wall through a platelet by means of the Faraday effect. The apparatus is shown in Figure 7. One of the magnets was inverted with respect to the other to align the magnetic spins in one side of the crystal opposite to those in the other side, thus creating two domains separated by a mutual wall. The magnetic flux through the crystal could be varied by changing the distance between the crystal and the magnets. (Each of the magnets had a flux density of 2400 gauss between its poles.) Figure 8a shows a $YFeO_3$ platelet containing an unperturbed straight domain wall, and Figure 8b shows another in which the domain wall has been moved across a crystal defect (not visible), and has become "hung up" on the defect. Yttrium orthoferrite platelets, grown from both the BaO-based solvent and a PbO-based solvent, have been compared by means of the straight domain wall apparatus. For similar crystal platelets, relatively free of voids, grain boundaries, crystals grown from the BaO-based solvent proved to be better than those from the PbO-based solvent, based on the ease with which a domain wall could be moved through the crystal.

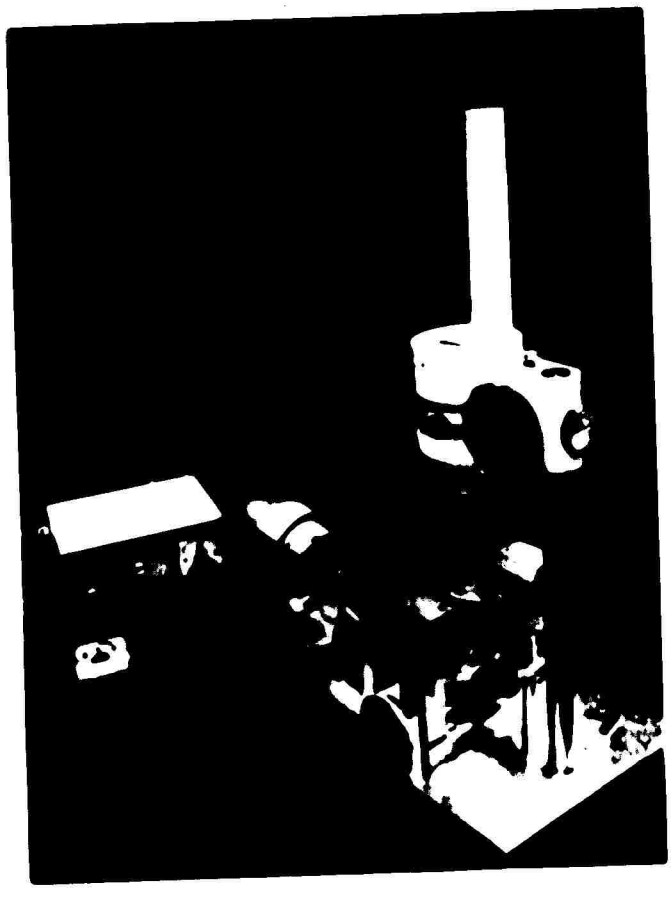

Figure 7. Straight Magnetic Domain Wall Apparatus

Figure 8a. Straight Magnetic Domain Wall in $YFeO_3$. 30X

Figure 8b. Defect Interaction with Magnetic Domain Wall in $YFeO_3$. 30X

## 3.5. Generation and Observation of Bubbles

### 3.5.1. Coercivity Measurements

The ultimate test of the single crystal material is the ease with which magnetic "bubbles" can be created and moved through a platelet, and experiments have been initiated to generate these bubbles and to measure the coercivity of the material and the mobility of the domain walls. Cylindrical domains are stable in a bias field of ~20 gauss, which is provided with an external magnetic coil, and they can be generated from the serpentine domains shown in Figure 9 by means of a pulsed magnetic field caused by current pulses through a small conducting loop placed in contact with the platelet. Any strip domains passing through this loop are cut and become cylindrical under the influence of the bias field. The bubbles can be moved quite easily over the surface by applying a magnetic gradient. An array of bubbles will align itself in a hexagonal pattern as shown in Figure 10. The coercive force can be deduced from this array (neglecting edge effects) with the aid of the relation[43]

$$\frac{H_C}{4\pi M_s} = \frac{3\pi r_o^3 h}{8\ell_{12}^4} \qquad (8)$$

where $H_C$ = coercive force,

$4\pi M_s$ = saturation magnetization,

$r_o$ = bubble radius,

h = thickness of the platelet, and

$\ell_{12}$ = distance between centers of an equilibrium array of bubbles.

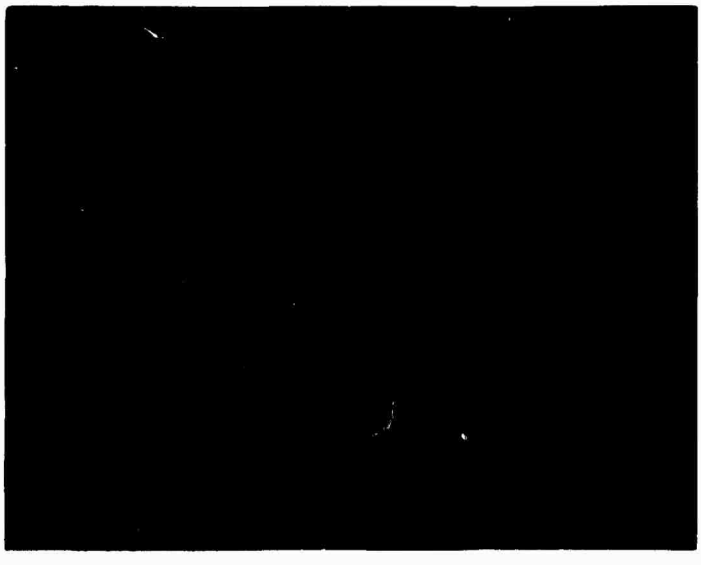

Figure 9. Serpentine Magnetic Domains in $YFeO_3$ (50X).

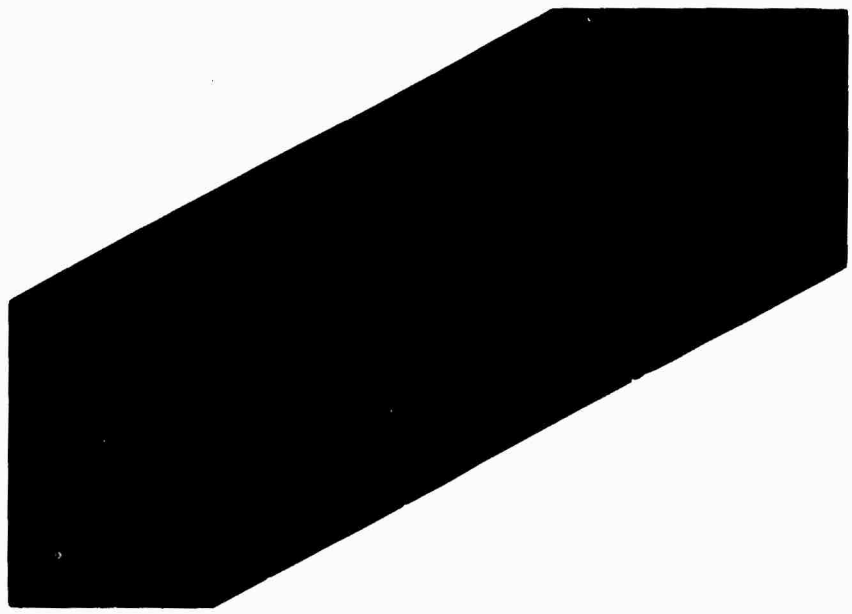

Figure 10. Array of Cylindrical Magnetic Domains in $YFeO_3$ Grown from $BaO-B_2O_3-BaF_2$ (Large Circle is the Bubble Generator). 31X.

The coercive force determined in this fashion for a polished $YFeO_3$ platelet grown in the barium-based solvent has been found to be ~0.05 Oe, which is comparable to the best values reported for crystals grown from the PbO-based flux after post growth annealing treatments,[44] and is well below the maximum acceptable limit of ~0.5 Oe for bubble domain devices.

3.5.2. Mobility Measurements[45]

Domain wall mobility is related to the velocity of a magnetic domain wall under the influence of a magnetic field by the equation (neglecting coercive force contributions)

$$V = \mu B \tag{9}$$

where V = wall velocity,

$\mu$ = mobility, and

B = magnetic field strength.

Let us consider a cylindrical domain of radius $r_o$ and apply two external magnetic fields, one a steady dc field and the other a pulsed field through the loop described in Section 3.5.1. There are now four contributions to the magnetic field, B:

$B_{pulse}$ = the magnetic field created by the pulse of current through the loop;

$B_{applied}$ = the applied dc magnetic field that maintains the bubble;

$B_{self}$ = the average magnetostatic energy at the wall of the bubble;

$B_{wall}$ = the equivalent magnetic field derived from the tendency of a magnetic domain wall to reduce its energy by reducing its area.

$B_{self}$ is given by

$$B_{self} = \mu_o M \cdot \frac{2}{\pi}\left[-\frac{2r_o}{h} + \sqrt{1+(2r_o/h)^2}\;\; E\left(\left(1+(h/2r_o)^2\right)^{-1}\right)\right] \qquad (10)$$

where E = the complete elliptic integral of the second kind,

$\mu_o = 4\pi \times 10^{-7}$,

M = magnetization, and

h = thickness of the platelet.

$B_{wall}$ is given by

$$B_{wall} = \frac{\sigma}{2r_o M} = \frac{\mu_o M \ell}{2r_o} \qquad (11)$$

where $\sigma$ = domain wall energy/unit area

$\ell$ = characteristic length of the material = $\sigma/\mu_o M^2$

The velocity now becomes

$$V = \frac{-dr_o}{dt} = \mu(B_{pulse} + B_{applied} - B_{self} + B_{wall}), \qquad (12)$$

which can be rearranged to give

$$\mu dt = \frac{-dr_o}{B_{pulse} + B_{applied} - B_{self} + B_{wall}} \qquad (13)$$

Integrating, and assuming that $B_{pulse}$ is applied just long enough to collapse the bubble, we get

$$\mu\Delta t = \int_{r_o}^{r_c} \frac{-dr_o}{\left[B_{pulse} + B_{applied} - B_{self} + B_{wall}\right]} \qquad (14)$$

where $r_c$ = the radius of the bubble at collapse.

Using the parameter $x = 2r_o/h$, we obtain from Eqs. 10, 11, and 14

$$\mu \Delta t = \int_{2r_c/h}^{2r_o/h} \left[ \frac{h}{2\mu_o M} \frac{dx}{\frac{B_{pulse} + B_{applied}}{\mu_o M} - \frac{2}{\pi}\left[ -x + \sqrt{1+x^2}\, E\left(\frac{1}{1+1/x^2}\right) + \frac{\ell}{h} \cdot \frac{1}{x} \right]} \right]. \tag{15}$$

All the quantities on the right hand side of this equation are experimentally measurable, as is $\Delta t$, the duration of the pulse, and the equation can be evaluated numerically for $\mu$.

The mobility has been measured by this technique for a polished (but otherwise untreated) $YFeO_3$ platelet grown from the $BaO\text{-}B_2O_3\text{-}BaF_2$ solvent, and has been found to be 2065 cm/sec Oe, which is again comparable to the best values reported for crystals grown from the PbO-based solvent.[44]

## 3.6. X-Ray Topographic Studies

Lang topographs have proven very useful for investigating the interaction between crystal defects and magnetic domains[46] as well as to reveal certain types of defects which are optically invisible, such as dislocations. Figures 11a, b show a portion of a $YFeO_3$ platelet (flat surface perpendicular to the c-axis) as seen in optical transmission and by Lang topographic techniques. The specimen was 0.04 mm thick, and the X-ray topograph was taken with Mo radiation (50 kV, 25 ma), and was exposed for 18 hours. A number of dislocations can be seen in the left half on the crystal as well as along the upper edge. The black spots in the right lower center in Figure 11b appear to be either precipitates

or inclusions, or possibly dislocations, which are not visible under optical microscopy. Further studies are needed to determine the exact nature of these defects and their interaction with the domains. Portions of the crystal, such as the upper right portion in Figure 11 appear to be quite defect-free.

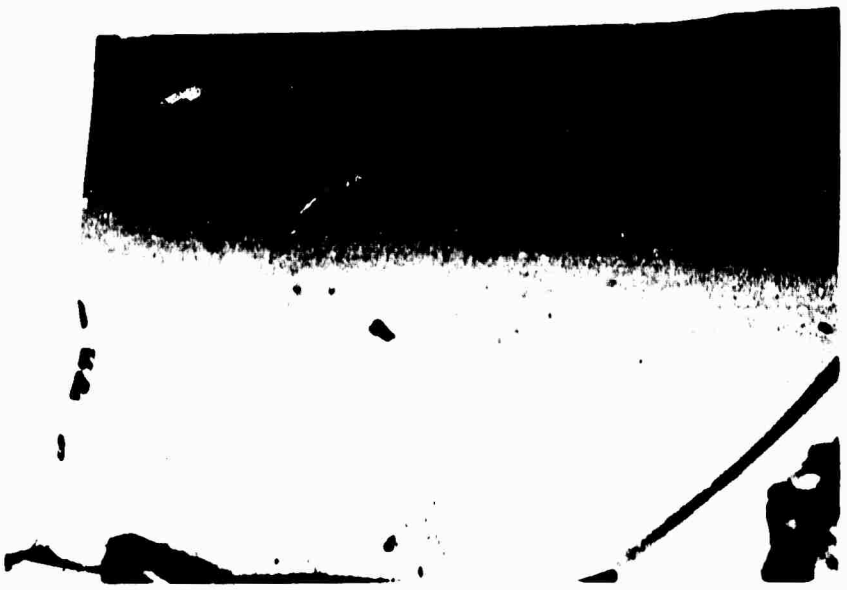

Figure 11a. Transmission Picture of Portion of $YFeO_3$ Platelet (100X).

Figure 11b. Lang Topograph of Same Area as Figure 11a. (100X).

## 4.0. PROCESS TECHNOLOGY

### 4.1. Cutting and Surface Preparation

Single crystals obtained from the growth process are oriented by use of a magnetic field so that they can be sliced into wafers perpendicular to the direction of easy magnetization (the c-axis). All cutting is done with a wire saw to produce slices, which are then mounted in plastic and lapped with 3 micron alumina, followed with 1 micron alumina to remove the 3 micron damage. Final polishing is done with Siton, a colloidal dispersion of $SiO_2$ in a basic medium, which removes essentially all surface damage. This process is repeated for the other side of the slice to produce a polished platelet of the desired thickness.

The extent of mechanical surface damage can be determined at each stage of the process by Laue back reflection x-ray patterns. Lattice distortions appear as smeared spots in these pictures. Figures 12a, b, c, show Laue patterns for the as-grown crystal, the as-cut slice from this crystal, and the same surface after the Siton polish, which restores the surface to its original undistorted condition, as far as can be determined from the Laue patterns.

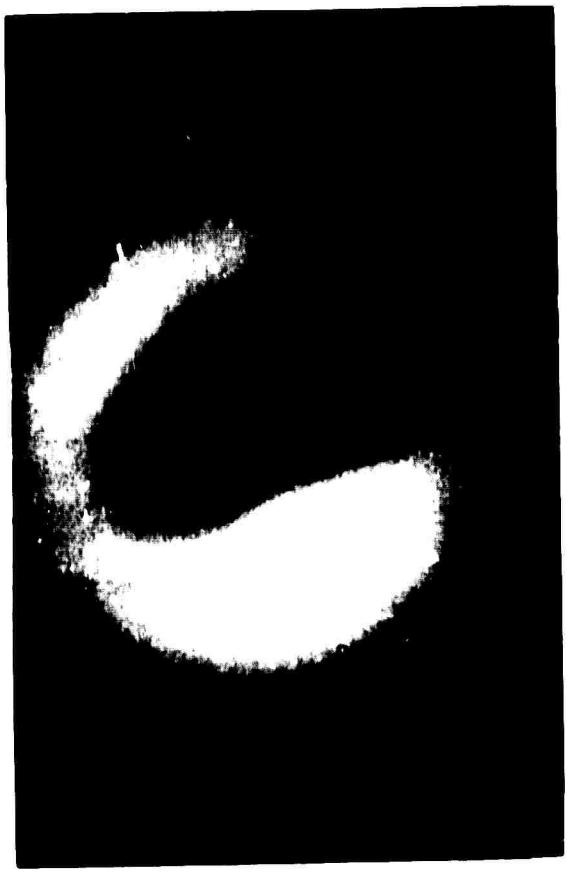

Figure 12a. As Grown Crystal $YFeO_3$.

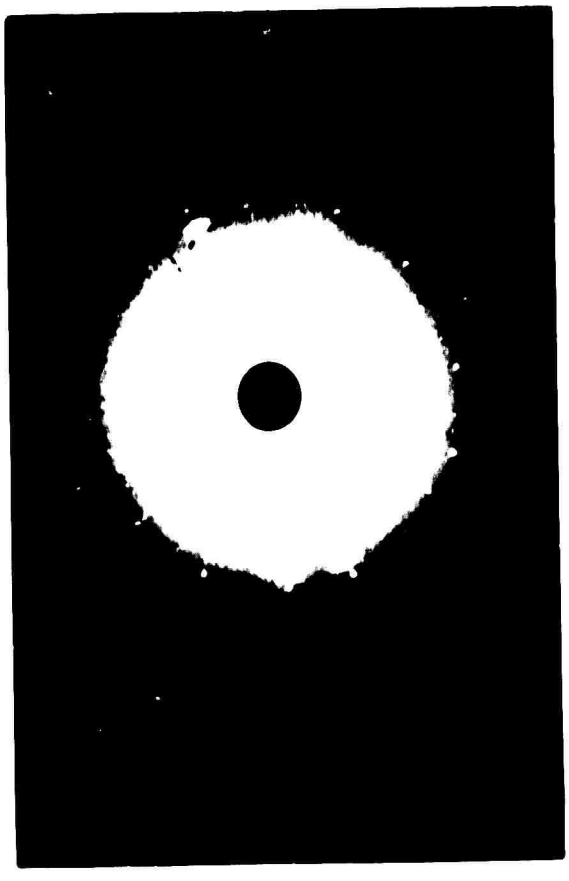

Figure 12b. As Cut Crystal

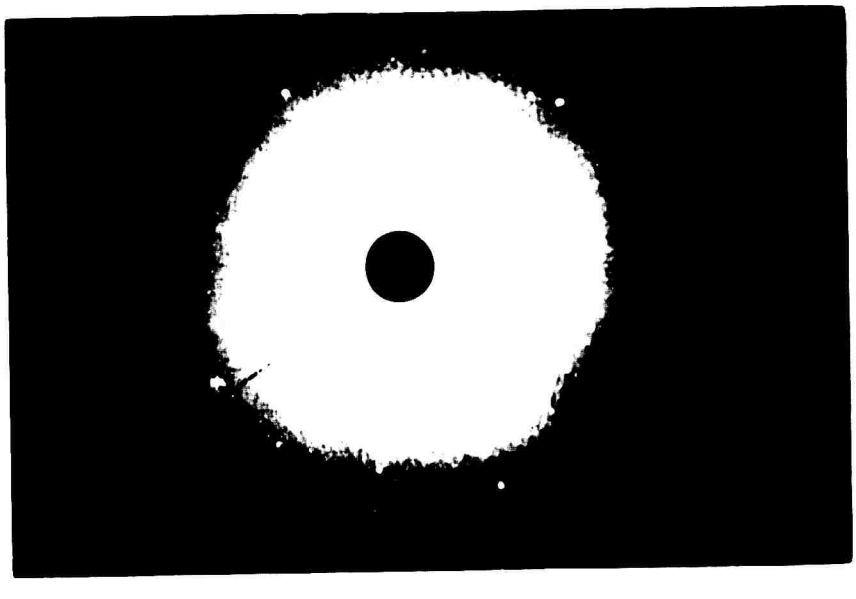

Figure 12c. Crystal After Polishing (Apparent Grains are a Film Artifact).

4.2. Chemical Etching

Both a selective and a nonselective etchant are required for characterization and evaluation of the orthoferrites. A nonselective etchant (chemical polishing agent) is needed to produce polished surfaces free of mechanical damage which occurs on handling and while slicing the crystals during processing. Once a platelet has been chemically polished, a selective etchant can be used to etch "grown-in" crystal defects such as grain boundaries and dislocations. Belt[47] has indicated that $Y_3Fe_5O_{12}$, which is considered to be similar to $YFeO_3$, can be either selectively or nonselectively etched with $H_3PO_4$ at 100-200°C for 10-45 minutes. Kurtzig[48] has found $H_3PO_4$ at ~ 160°C to be effective in removing surface damage from $YFeO_3$, but did not find a proper chemical polish.

To evaluate phosphoric acid as an etchant for $YFeO_3$, 85% $H_3PO_4$ was heated to various temperatures (100-442°C) in a platinum crucible, and after 10-30 minutes at temperature to allow the acid to come to equilibrium the etching was performed. Equilibrium was especially important at temperatures above 213°C since the $H_3PO_4$ loses $H_2O$ at this temperature to form $H_4P_2O_7$.[49] It has been found that at temperatures of 160-170°C dislocation etch pits are formed in approximately 30 minutes, and at 400°C chemical polishing in completed in ~ 1.5 minutes. The chemical etching procedure is in agreement with Belt and Kurtzig, except that Kurtzig reports a removal rate of 1 micron per minute, whereas we find a removal rate of ~ 0.04 micron per minute for the {001} plane. In addition, a very effective chemical polishing procedure has been found at the higher temperature.

## 5.0. CONCLUSIONS

It is appropriate at this point to evaluate the work performed during the first six months of this project in the light of other competing techniques and materials for the fabrication of magnetic bubble devices. It is especially pertinent to evaluate the potential that this particular avenue of investigation offers for minimizing the effort devoted to the final selection of material and method of fabrication for such devices.

We have thus far demonstrated the feasibility of controlled solution growth of high quality $YFeO_3$ crystals in a novel solvent that is superior in several respects to conventional solvents. The merits of the $BaO\text{-}B_2O_3\text{-}BaF_2$ solvent have been contrasted with the problems associated with the PbO-based solvents in the body of this report, and need no further elucidation here. Let us rather concentrate on the possibilities that further development of this solvent offers. Perhaps the most important is the evaluation of liquid phase epitaxy as a practical growth technique for magnetic rare earth compounds. Heretofor, investigations have been hampered by the corrosive and volatile nature of the PbO-based solvents, and by the tendency of these solvents to attack the substrate.[50] The BaO-based solvent should at least alleviate if not obviate these problems in order to permit the more fundamental problems of epitaxial growth to be studied.

Why is steady-state liquid phase epitaxial growth to be preferred over various other techniques for the growth of bubble materials which have been reported recently, such as Bridgman growth from the melt

id the floating zone technique? These methods permit the rapid
rowth of large sound crystals of $YFeO_3$, but the crystals are of the
rong geometry for device use (requiring thin platelets normal to the c-axis),
nd a great deal of processing is necessary to produce polished thin platelets
f the proper orientation.

Perhaps a more important consideration is that it is very difficult to
ontrol the homogeneity of complex crystals, such as the mixed cation garnets,
y these melt techniques. In addition, the bubble garnets are needed in
hicknesses of the order of a few microns, and it is extremely difficult to
ut and polish or even handle these materials when they are of this thickness.

Solution growth offers the advantage of being able to precisely control
omogeneity in a mixed cation crystal, particularly if the growth is isothermal
as in the steady-state technique. Even though growth rates are orders of
magnitude slower than those for melt growth, control of geometry in solution
growth obviates the need for extensive processing which consumes time and
wastes material. The combination of steady-state solution growth with our
stable solvent should shorten the path toward the optimum crystal growth
process, which appears to be liquid phase epitaxy.

We turn now to the choice of material for bubble devices. At present
the uniaxial garnets appear to be the most promising, but the origin of their
uniaxiality is unknown, and may in fact, be induced by their nonisothermal
mode of crystal growth. One feature of the steady-state growth technique
developed here is its usefulness over a wide range of temperature (850-> 1400°C)

without change in the stability of the solvent or equipment. This permits critical questions to be examined about the nature of uniaxiality in the garnets. For example, can uniaxial garnets be grown by a steady-state technique, either above or below 1200°C (the point at which garnets appear to lose uniaxiality), or is slow cooling a necessary requirement? If it is, of course, the uniaxiality would not be an intrinsic property of the crystal, lessening the attractiveness of the garnets for device use. While this question is being resolved, the development of growth techniques should logically be restricted to materials which are fairly well characterized, such as $YFeO_3$.

In conclusion, the steady-state solution growth technique, at this time, offers the broadest possible base for exploring solution growth, both homoepitaxial and heteroepitaxial, of both garnets and orthoferrites, and thus may offer the shortest path to eventual device fabrication.

## 6.0. FUTURE PLANS

1. The properties of the barium-based solvents will be explored further, including $BaO-B_2O_3$ with additions of $BaF_2$ and other barium halides. Properties to be measured include phase equilibria, density and solvent power of these solvents, as well as their propensity for the growth of high quality crystals.

2. Crystal growth parameters in the steady-state system will be varied in an effort to better understand and optimize the growth process. The parameters to be investigated are the solvent composition, the interface temperature, temperature gradient at the interface, stirring rate in the liquid, and the source to seed distance.

3. Epitaxial growth of $YFeO_3$ on large areas will be attempted using $YAlO_3$ substrates.

4. Characterization of the single crystals will receive more emphasis as additional crystals become available. The characterization studies will include etch pit studies, measurement of bubble domain coercivity and mobility, light and dark field transmission microscopy to determine the nature of defects, Lang topography to observe dislocations and other optically invisible defects, emission spectrographic analysis to determine the amount of barium incorporation in the lattice, and careful measurements of optical absorption spectra of the polished platelets, which can be used to deduce the presence of solvent ions in the crystal.[51]

Precise characterization will permit sensible adjustment of crystal growth parameters to optimize the system. Annealing studies will be carried out to clarify recent work[52] on the enhancement of coercivity and mobility of $YFeO_3$ by a 1000-1200°C anneal.

5. In addition to $YFeO_3$, the growth of other magnetic bubble materials, such as the mixed garnets, will be attempted in the steady-state unit.

## APPENDIX

### 7.0. Phase Relations in PbO-Based Solvents

Existing literature data for crystal growth in this system allow several conclusions to be drawn. The solvent has been different in many cases and most often has been a mixture of $PbO-PbF_2-B_2O_3$. Garnets have most often been grown from this solvent. YIG is incongruently melting and its phase field in the "pseudo-ternary" system ($Fe_2O_3-Y_2O_3$-solvent) lies close to the $Fe_2O_3$-solvent join, quite far removed from the YIG-solvent join. This is not the case with the congruently melting $YFeO_3$, and its stability regime includes the $YFeO_3$-solvent join. In fact, the $YFeO_3$-solvent system can probably be treated as a quasibinary for all the solvent mixtures of interest. This implies that the maximum liquidus temperature and minimum liquidus slope for the $YFeO_3$ phase field lies along the $YFeO_3$-solvent join, that there is probably a quasi-eutectic reaction close to the solvent apex of the composition triangle and that the slope of the liquidus surface is a minimum along this join.

$Fe_2O_3-Y_2O_3-PbO$ is the simplest ternary, and has been partially investigated by Nielsen and Dearborn.[53] The estimated liquidus projection for this system is shown in Figure 13. The isotherms are known at the $PbO-Fe_2O_3$ and $Fe_2O_3-YFeO_3$ binary joins and are estimated along the third side of the composition triangle (by analogy

with PbO - $La_2O_3$, $Sm_2O_3$, $Gd_2O_3$ ).[54] In addition, Nielsen and Dearborn [53] data for the liquidus projection in the region close to the $Fe_2O_3$-PbO binary are used. Temperatures along the $YFeO_3$-PbO quasibinary join can be estimated from the equation

$$x = x_o e^{-\Delta H/RT}, \qquad (16)$$

where $x$ = mole fraction $YFeO_3$,

$x_o$ and $\Delta H$ are constants assumed independent of temperature over a fairly wide range,

$R$ = gas constant, and

$T$ = absolute temperature.

An expression of this type is commonly used to represent liquidus curves in binary compound systems, and it is assumed that when the compound dissolves in the melt it dissociates completely. Since $x = 1$ at $T = 1670°C$, and we can assume a eutectic at $x \sim 0.05$, $T \sim 600°C$ (the exact position is not too important), the constants are fixed at $x_o = 100$ at. fr. and $\Delta H = 18,000$ cal/mole. Equation 15 can now be used to generate liquidus points along the quasi-binary which lead to the isotherms shown in Figure 13. The qualitative liquidus surface agrees with all existing crystal growth data for the $Fe_2O_3$-$Y_2O_3$-PbO system. An analogous liquidus projection (Figure 14) can be drawn for the $Fe_2O_3$-$Y_2O_3$-PbO/$PbF_2$/$B_2O_3$ system with the added complication of a YOF phase which often appears during crystal growth of $YFeO_3$.

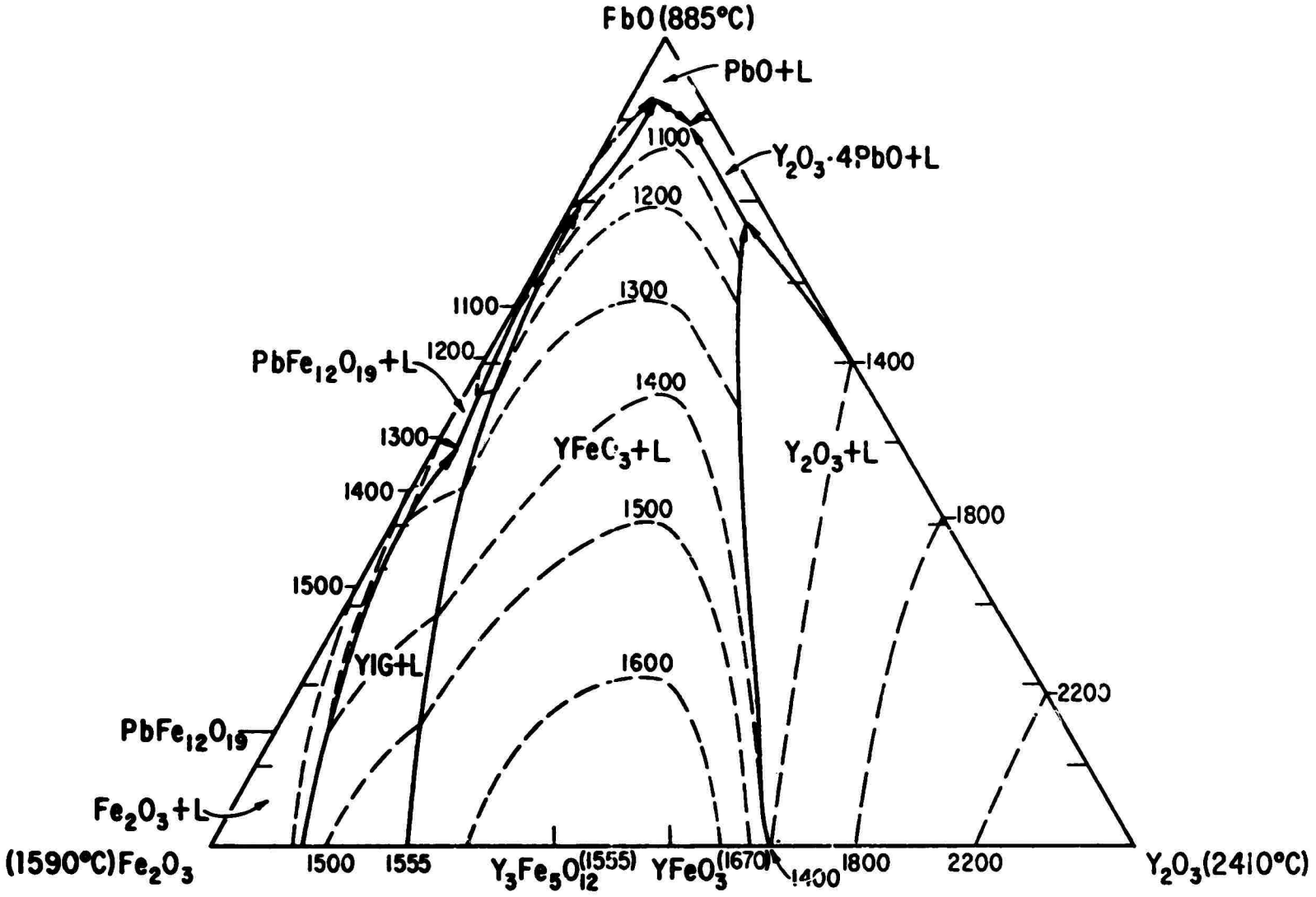


Figure 13. $Fe_2O_3$-$Y_2O_3$-PbO System Extimated Liquidus Projection and Isotherms.

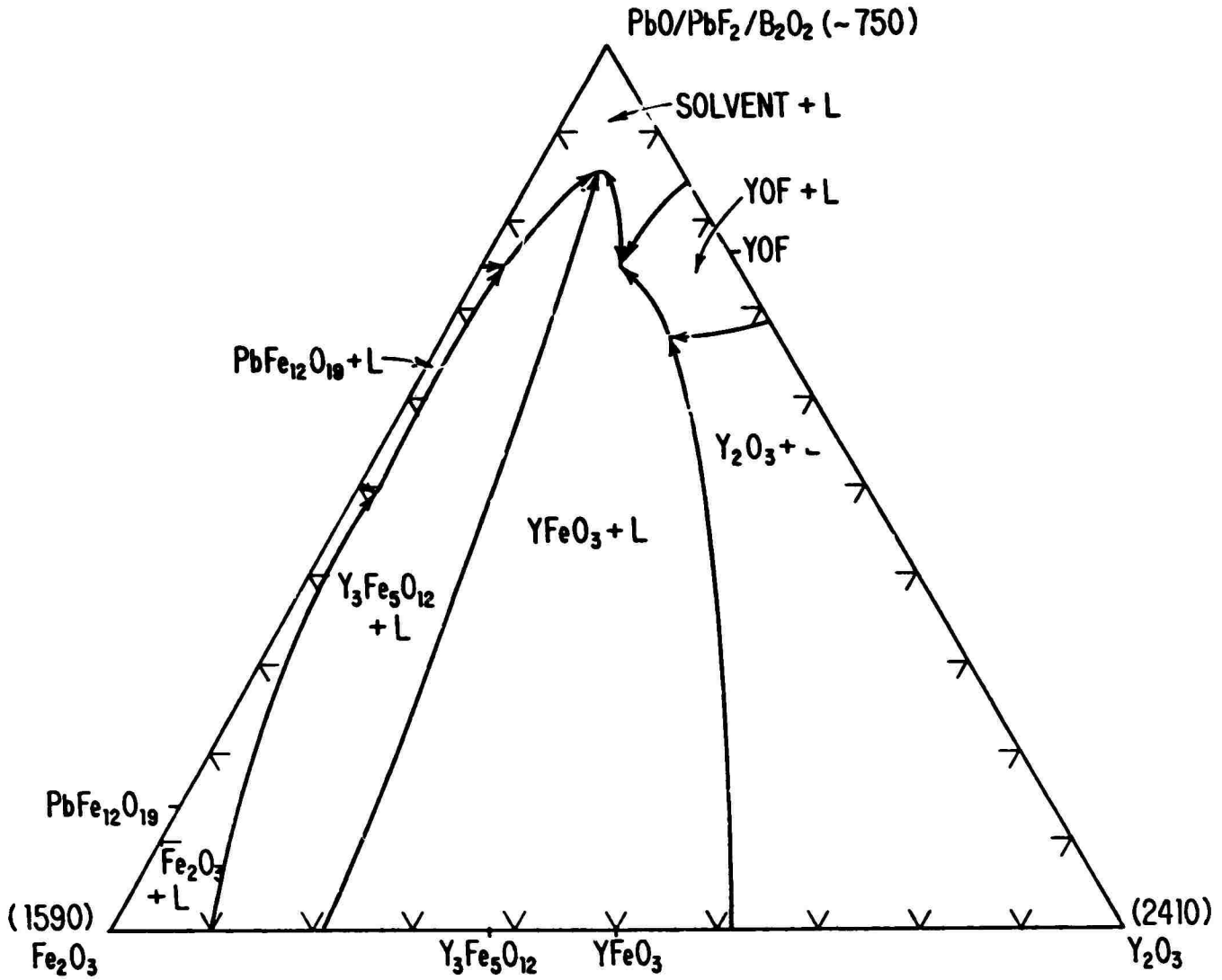


Figure 14. $Fe_2O_3$-$Y_2O_3$-PbO/$PbF_2$/$B_2O_3$ System Possible Liquidus Projection

## REFERENCES


1. A. H. Bobeck, Bell Syst. Tech. J. 46, 1901 (1967).

2. L.G. Van Uitert, D.H. Smith, W.A. Bonner, W.H. Grodkiewicz and G.J. Zydzik, Mat. Res. Bull. 5, 455 (1970).

3. L.G. Van Uitert, W.A. Bonner, W.H. Grodkiewicz, L. Pictroski, and G.J. Zydzik, Mat. Res. Bull. 5, 825 (1970).

4. J.P. Remeika, J. Am. Chem. Soc. 78, 4259 (1956).

5. R.C. Linares, J. Am. Ceram. Soc. 45, 307 (1962).

6. R.C. Linares, R.B. McGraw and J.B. Schroeder, J. Appl. Phys. 36, 2884 (1965).

7. M. Kestigian, J. Am. Ceram. Soc. 50, 165 (1967).

8. E.D. Kolb and R.A. Laudise, 16th Annual Magnetism and Magnetic Materials Conference, 1970.

9. G.A. Bennett, J. Cryst. Growth 34, 458 (1968).

10. M. Sparks, B.R. Tittman, J.E. Mee, and C. Newkirk, J. Appl. Phys. 40, 1518 (1969).

11. W.H. Grodkiewicz, E.F. Dearborn and L.G. Van Uitert, Crystal Growth, Ed. H.S. Peiser, 441, Pergamon Press, New York (1967).

12. T. Okada, K. Matsumi and H. Makino, International Ferrite Conference, Kyoto, Japan, 1970.

13. S. Blank, L.K. Shick and J.W. Nielsen, 16th Annual Conference on Magnetism and Magnetic Materials, 1970.

14. D.C. Doughty and E.A.D. White, Acta Cryst. 13, 761 (1960).

15. E.A. Giess, D.C.Cronemeyer, L.L. Rosier, and J.D. Kuptsis, Mat. Res. Bull. 5, 495 (1970).

16. J.W. Nielsen, 16th Annual Magnetism and Magnet. Materials Conference, 1970.

## REFERENCES


17. H.J. Van Hook, J.Am. Ceram. Soc. 44 208 (1961).

18. Ibid., 45, 162 (1962).

19. W. Tolksdorf, J. Crystal Growth 3, 4, 463 (1968).

20. G.F. Reynolds and H.J. Guggenheim, J. Amer. Chem. Soc. 65, 1655 (1961).

21. R. A. Laudise, "The Art and Science of Growing Crystals," p. 252 J.J. Gilman, Ed., John Wiley & Sons, New York (1963).

22. R.A. Laudise, R.C. Linares and E.F. Dearborn, J. Appl. Phys. 33 Suppl. 1362 (1962).

23. R.C. Linares, J. Appl. Phys. 35, 433 (1964).

24. R.C. Linares, J. Am. Ceram. Soc. 48, 68 (1965).

25. S.H. Smith and D. Elwell, J. Crystal Growth 3, 4, 471 (1968).

26. J.W. Nielsen and E.F. Dearborn, J. Phys. Chem. Solids 5, 202 (1958).

27. J.W. Nielsen, P 2,957,827, filed April 30, 1957.

28. B.M. Wanklyn, J. Crystal Growth 5, 323 (1969).

29. E.A. Giess, J. Am. Ceram. Soc. 49, 104 (1966).

30. L.G. Van Uitert, R.C. Sherwood, W.A. Bonner, W.H. Grodkiewicz, L. Pictroski and G. Zydzik, Mat. Res. Bull. 5, 153 (1970).

31. H.H. Quon and A.G. Sadler, J. Can. Ceram. Soc. 36, 33 (1967).

32. J.S. Berkes and W.B. White, J. Cryst. Growth 6, 29 (1969).

33. J.W. Nielsen, J. Appl Phys. 31, 515 (1960).

34. L. Brewer, Natl. Nuclear Sci. Ser., Div. IV, 19B, p. 13.

35. W.A. Tiller, J. Cryst. Growth 2, 69 (1968).

36. C.B. Oliver, J. Electrochem. Soc. 112, 629 (1965).

## REFERENCES


37. J.W. Nielsen, J. Appl. Phys. 31 Suppl. 51 (1960).

38. D.C. Leo, R.F. Belt, and D.A. Lepore, Final Report, Manufacturing Methods for Growing Large Sound Yttrium Iron and Yttrium Gallium Iron Garnets, Contract No. AF33(615)5366, AFM-TR-68-298, June 1968.

39. S. Geller, Acta Cryst. 11 565 (1968).

40. J.P. Remeika and T.Y. Kometani, Mat. Res. Bull. 3, 985 (1968).

41. H.T. Evans, B.E. Appleman and D.S. Handwerker, presented at the annual meeting of the Am. Crystallographs Assoc., March 28, 1963, Cambridge, Mass. pp. 42-43.

42. D. Treves, J. Appl. Phys. 36, 1033 (1965).

43. A.H. Bobeck, R.F. Fischer, A.J. Perneski, J. P. Remeika and L.G. Van Uitert, IEEE Trans. on Magnetics MAG-5 544 (1969).

44. F.C. Rossol, Phys. Rev. Letters 24, 1021 (1970).

45. R. Lacey, private communication.

46. A.J. Kurtzig and J.P. Patel, Phys. Letters 33A , 123 (1970).

47. R.F. Belt, J. Appl. Phys. 40, 1644 (1969).

48. A.J. Kurtzig, Technical Report No. 5405-1, Contract NONR-225 (83, May 1968.

49. "Handbook of Chemistry and Physics," 37th Edition, Charles D. Hodgman, Ed., Chemical Rubber Publishing Co., p 561, (1955).

50. L.K. Shick and J.W. Nielsen, Presented at the 16th Conference on Magnetism and Magnetic Materials, Miami, Florida, 1970.

51. D.L. Wood, J.P. Remeika and E.D. Kolb, J. Appl. Phys. 41, 5315 (1970).

52. D. L. Portigal, 16th Annual Conference on Magnetism and Magnetic Materials, 1970.

53. J. W. Nielsen and E. F. Dearborn, J. Phys. Chem. Solids 5, 202 (1958).

54. E. M. Levin, C. R. Robbins and H. F. McMurdie, "Phase Diagrams for Ceramists", the American Ceramic Society, Inc. 1969.